

Calorimetric Sensors

Richard E. Cavicchi
Chemical Science and Technology Laboratory
National Institute of Technology
Gaithersburg, MD 20899
301 975 3970
FAX 301 975 2643
rcavicchi@nist.gov

Summary

The calorimetric gas sensor has evolved from a simple metal hot wire to a modern device fabricated using micromachining techniques. The principle of operation is to detect the heat evolved from combustible gases on the sensor surface. While the most widely used device is still the discrete catalyst-coated platinum coil known as the pellistor, considerable research has taken place in the last two decades to produce miniature devices that use less power and provide greater measurement capability. These devices have separate heater and temperature control, can be fabricated as arrays, and operated with time-varying signals that produce data that can provide information about chemical composition. The technology for miniaturization of calorimetric devices is also finding new applications in the area of biosensors. This review includes an introduction to calorimetric gas sensors, a review of new thin film structures, catalyst materials, catalyst poisoning effects, new signal operating modes, packaging, biological sensors, and device applications.

Table of Contents

1. Introduction
2. Catalytic Bead Devices
3. Thin film and MEMS Devices
4. Materials
5. Poisoning
6. Signal Analysis and Operating Modes
7. Packaging
8. Applications
9. Safety
10. Conclusions

1. Introduction

The calorimetric gas sensor is a gas sensor that uses calorimetry as the transduction principle, by measuring the heat of a reaction on the sensor surface. This class of devices, in various configurations is also known by the names “pellistor,” “catalytic bead,” “catalytic gas sensor,” “combustible gas sensor,” or “thermometric gas sensor.” The calorimetric gas sensor is one of the earliest portable gas sensors. The devices were developed in the 1950’s for the safety application of detecting methane in coal mines.

The first calorimetric gas sensors were made as a simple coil of Pt wire. A current applied through the wire heated the Pt to 900 °C to 1000 °C, which was hot enough to sustain combustion on the Pt surface in the presence of a flammable gas mixed with air. The exothermic nature of the combustion caused a rise in the temperature of the Pt wire, causing a change in the Pt wire's resistance. External circuitry was used to measure this change in resistance. The Pt wire thus performed three functions: heater, catalytic surface for combustion, and thermometer. While the device was very simple to fabricate and operate, the high temperatures caused evaporation of Pt from the wire, and therefore drift and early failure of the devices.

In the 1950s work to improve the portable flammable gas detector was carried out in the U.K. by the Safety in Mines Research Establishment. In particular, the 1959 patent submission by Alan Baker through the National Research Development Corporation describes for the first time the device configuration which is most widely used today (Baker, 1962). The key idea was to apply an oxide supported catalyst to the Pt wire, which then only performs the functions of heater/thermometer as shown in Figure 6-1. The oxide-supported catalyst has a higher catalytic activity and can operate at lower temperatures (300 °C to 500 °C), with better resistance to poisoning. The lower temperatures in turn enhance the lifetime and reduce dramatically the drift problems for the Pt wire heater. Devices of with this configuration are often referred to as "pellistors" or "catalytic bead devices."

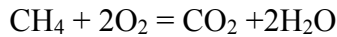
The calorimetric gas sensor, by its essential transducing principle, finds applications for the combustible gas detection sector of the chemical sensing market. In addition to the application for detecting methane levels in mines, these sensors are also used for petroleum drilling and processing facilities, propane filling facilities, automotive fuel systems, liquid or gas heating systems, sewer and manhole monitoring, and methane stripping plants for landfills. The world market for combustible gas sensors was \$374 million in 2005, of which catalytic gas sensors (Frost, 2006) represent 55 percent. The largest competing technology in the combustible gas sensing market is the infrared sensor.

Calorimetric gas sensors will detect the presence of any combustible gas as long as oxygen is also present for the necessary reaction to take place. For safety applications, this is sufficient, even without a capability for species identification. Units are commonly calibrated in terms of a percentage of the lower explosive limit (LEL) of the gas that is expected to be measured in the application. For example, a reading of 10 % LEL for methane corresponds to a concentration of methane in air that is ten percent of the LEL, which is 5 % by volume, thus a net concentration of 0.5 % by volume. Detailed tables of the concentration for the LEL for a variety of gases have been published (Firth et al., 1973).

Advantages of calorimetric gas sensors include low sensor cost, small size and portability, low power consumption, established utility in a decade's market, and long operating life. The chief drawbacks are the susceptibility to poisoning of the catalyst when certain gases are present, and the need for recalibration. In many applications for

combustible gas sensing, the more expensive infrared sensing technology is making inroads, where contamination of the sensor is an issue, frequent calibration is costly or difficult, and small sensor size is not a requirement. Semiconductor gas sensors also are used to detect combustible gases. These devices are the lowest cost, but have the drawback of detecting some non-combustible gases and thereby creating false alarms. The largest usage of the semiconductor sensors for combustible gas detection is for handheld leak detection instruments. Table 1 provides some comparisons of the catalytic, infrared, and semiconductor sensing technologies as applied to combustible gas detection.

A number of excellent reviews of calorimetric gas sensor technology have been published (Jones, 1987, Walsh and Jones, 1991, Miller, 2001, Bársony et al., 2009). The fundamental aspects of the device operation are well described in these reviews and will only be summarized here. As an example, the combustion of methane on a catalyst surface produces reaction products of water and carbon dioxide:



where the enthalpy change of combustion ΔH for one mole is -890 kJ. Thus the excess power ΔP given by a reaction rate dr/dt (moles of reducing gas being oxidized per second) is

$$\Delta P = dr/dt \Delta H$$

The reaction rate depends on the flow of reactant over the sensor, the temperature of the sensor, the exposed surface area with catalyst, and the reaction kinetics of the catalyst and reacting reducing gas. In the most common implementation, using a pellistor, the signal is the change in the heater resistance. The pellistor is typically mounted in a Wheatstone bridge circuit as shown in Figure 6-2 (a). The circuit includes a pellistor activated with catalysts with resistance R_s , and a pellistor without catalyst with resistance R_r that serves to compensate for variations in the background temperature and/or flow. The output voltage of the Wheatstone bridge is given by

$$V_{\text{out}} = V_{\text{in}} [R_s / (R_s + R_r) - R_1 / (R_1 + R_2)]$$

In the absence of the reducing gas, both the activated device and the compensator are supplied with sufficient current to heat the two devices to the same elevated temperature. Resistors R_1 and R_2 are tuned so that under this condition the bridge is balanced, with $V_{\text{out}} = 0$. Excess power ΔP produced by a reaction on the catalyst/oxide coating, causes an increase in the temperature of the device

$$\Delta T = \Delta P / K$$

where K is the thermal conductance of the pellistor to its environment at room temperature (a combination of conductive, radiative, and convective heat transfer.) This changes the resistance of the R_s by an amount

$$\Delta R = \beta \Delta T$$

where β is the temperature coefficient of resistance of the Pt heater. Assuming that in the absence of a gas signal at operating temperature T , $R_s(T) = R_r(T)$, and that $R_1 = R_2$, and assuming that in the presence of a combustible gas the resistance change $\Delta R/R_s \ll 1$, then combining results, the signal ΔV will be given by

$$\Delta V = \frac{V_{in}}{4R} \frac{\beta}{K} \frac{dr}{dt} \Delta H$$

It should be noted that this ΔV will give rise to a small change in the current through R_r , which will change the value of R_r , which depending on the device parameters and operating points may need to be accounted for. An alternative to work around this problem is to use a current source as the supply for the bridge. Another setup of the bridge would have R_r and R_s in separate branches of the bridge, i.e. exchange the places of R_r and R_1 in Figure 2, which works around this problem in the case of voltage driven operation. At higher concentrations, the constant supply modes of operation can result in elevated pellistor temperatures, which alter the reaction rate and makes the signal dependence stronger than linear. Use of a feedback network, in which the temperature of the sensor remains constant, avoids this issue. An example circuit is shown in Figure 6-2 (b). In this configuration, the operational amplifier will reduce its output in the presence of a combustible gas so that the loss of joule heating through the resistor matches the increase in dissipated power due to the reaction on the sensor's catalyst. The value of R_s will then remain unchanged. A second bridge with a compensating pellistor without catalyst may be used to provide a baseline that accounts for changes in ambient temperature and air flow rate.

This review will emphasize new developments in calorimetric gas sensor technology, the chief of which is the use of thin film and micromachining techniques to produce devices that are much smaller, consume less power, and can be fabricated in a batch mode at lower cost. The miniaturization brings additional advantages, such as the ability to fabricate arrays, and to perform rapid temperature modulations.

2. Catalytic Bead Devices.

The most widely available commercial calorimetric sensors are pellistors, or catalytic bead devices, as shown in Figure 6-1. The devices are fabricated by a method that involves hand-fabrication. The core of the devices is fabricated using Pt wire, which has the advantages of being robust at high temperatures and having a useful temperature coefficient of resistivity of $0.0038 (\Omega/\Omega)/^\circ\text{C}$. (By measuring the resistance of a Pt wire at two temperatures, and dividing the difference by the resistance at the lower temperature, the temperature change can be calculated by dividing that ratio by the temperature coefficient of resistance.) Fine wire, of diameter $10 \mu\text{m}$ to $50 \mu\text{m}$ is used, with the advantage of lower power consumption at lower thicknesses coming with the trade-off of greater device fragility. The Pt wire is wound by an automated tool into a coil

of precise dimensions. The Pt wire is coated with an alumina support material that is impregnated with a catalyst. The high effective surface area of this supported catalyst ensures that under diffusion-limited conditions, there is sufficient active catalyst for combustion, even if some of the catalyst has become inactive. This helps to ensure long operating life of the device. The coated device is fired to a high temperature (500 °C to 800 °C). The device is soldered into a package that may include filters and a flame arrestor.

Typical characteristics of commercial devices include the following performance parameters. Sensitivity is commonly listed as covering the range between zero and one hundred percent of the lower explosive limit, with a minimum sensitivity at around one to two percent of the LEL. Operating temperatures are in the range of 300 °C to 600 °C, with power consumption in the range of 0.2 W to 1 W. Response time is quoted as the time needed for the sensor to produce a signal that is within 90 % of its final value when exposed to a step change in the concentration of a test gas. Typical values for this parameter are 10 s to 15 s. The devices operate satisfactorily with an ambient temperature in the range -10 °C to 50 °C and over a wide range of relative humidity, up to the dewpoint. The devices typically are specified to last for three to five years, with an expected drift of around 10 percent per year. Exposure to poisoning agents reduces the lifetime.

3. Thin film and MEMS Devices

While conventional pellistor bead devices have found extensive use for combustible gas detection in mines and other industrial applications, there is a growing body of research pointing towards advantages that can be had from a MEMS (microelectromechanical systems, which is now in common usage to describe devices fabricated by thin film micromachining techniques) version of the device. MEMS devices generally will consume much less power, can be fabricated using efficient silicon planar methods at potentially lower cost, can be integrated with other sensors and electronics (such as multiplexing or preamplification stages), and because of their low thermal mass offer new sensing schemes based on rapid temperature modulation.

Earliest thin film versions of the calorimetric sensor include a design based on a Pt heater on an alumina substrate(Luo et al., 1991) (Makovos et al., 1993), a Pt heater with a separate thermometer on a micromachined SiN membrane(Gall, 1991), a Pt heater on a SiN membrane (Krebs and Grisel, 1993), and, in work that served as the seed for much of the following work, array sensors with varying time and temperature operation(Gall, 1993). Two designs for a micromachined version of a calorimetric gas sensor are shown in Figure 6-3, from Gall, (Gall, 1993). In Figure 6-3 (a), a single metal layer serves as the heater, temperature sensor, and catalyst. This is in close analogy to the earliest versions of the hot-wire calorimetric sensors. In Figure 6-3 (b), which requires additional process steps, the three functions of heating, thermometry, and catalysis are performed by separate structures. Zanini et al. reported enhanced performance using a dual micromachined device to reduce common mode signals due to changes in the ambient temperature and flow rate(Zanini et al., 1995). Figure 6-4 shows an example of data from

the device. A sensitivity of 8 $\mu\text{l/l}$ for propylene was achieved. An interesting oscillatory reaction was detected for CO at 300 °C for concentrations near 10ml/l. An example image of a simple MEMS calorimetric gas sensor is shown in Figure 6-5(Furjes et al., 2005). This device has a Pt meander heater and a supported Pt catalyst deposited on the surface of the sample, with a bare reference. The heater also acts as the thermometer, analogous to a conventional pellistor device.

In the fabrication of MEMS devices, the most commonly used material for the heater is Pt, due to its resistance to oxidation, stability at high temperature and thermal expansion compatibility with other layers. An adhesion layer of Ti of 10-20 nm is commonly applied prior to the Pt deposition. Polysilicon has also been used to fabricate heater elements(Manginell et al., 1996, Hierlemann and Baltes, 2003, Engel et al., 2004) (Cavicchi et al., 2004). It is often selected because it is a material that is used in conventional electronics fabrication, however, its temperature range (to 500 °C maximum) is less than Pt. Single crystal silicon has also been used(Furjes et al., 2002b, Furjes et al., 2002a). It has improved stability compared to polysilicon, and a larger temperature coefficient of resistance than platinum in the range 320 °C -550 °C(Furjes et al., 2002a).

Thermocouple junctions can also be used to sensitively measure the temperature (Cavicchi et al., 2004, Houlet et al., 2008). A thermocouple measures the voltage generated by the Seebeck effect, and consists of a junction between two dissimilar materials at the temperature to be measured, with a series connection to a second junction at a reference temperature. Example materials that have been used for the couples are polysilicon/Al(Cavicchi et al., 2004)Au- and boron-doped $\text{Si}_{0.8}\text{Ge}_{0.2}$ (Houlet et al., 2008), SnO_2/Al (Casey et al., 2003), and Bi/Cu (Park et al., 2009). The thermopile reference can be fabricated on the same suspended platform as the sample to reduce power loss and enhance signal as in the example of Figure 6-6(Cavicchi et al., 2004). Voltage applied to separate heaters for the sample and reference sides are tuned to minimize the thermopile voltage signal in the absence of a combustible gas. Sensitivities 3 mole/mole (3 ppm) of methanol in air were demonstrated.

Thermometry has also been accomplished with the use of thermoelectric materials, which develop a voltage in response to a temperature gradient. Shin et al. have developed a hydrogen sensor based on a thick film alkali-doped NiO thermoelectric film(Shin et al., 2003). The device was fabricated on an alumina substrate, with a Pt catalyst deposited on one side of the NiO film. Reaction of H_2 with the catalyst warmed the one side of the device, producing a thermoelectric voltage. The base operating temperature was set to 100 °C by mounting the device on a plate heater.

As the device size shrinks, temperature uniformity becomes an increasingly important issue, especially for methods that may utilize the difference in reaction rates as a function of temperature as a means of chemical selectivity. The temperature uniformity of the device becomes especially important if temperature modulation is to be used for chemical identification. A broad temperature distribution over the device leads to a broadening of

temperature signals, reducing the ability of the device to discriminate chemical reactions that have different turn-on temperatures. To improve the temperature uniformity of their device the width of the microheater may be varied over the surface. Thermal imaging is a useful technique to evaluate heat transport in these structures (Aigner et al., 1996, Lee et al., 2003, Cavicchi et al., 2004, Furjes et al., 2002a, Furjes et al., 2005). Figure 6-7 shows an example where the microheater is narrowest at the outermost region of the device (where the thermal conductance to the background temperature is the largest) becoming progressively wider as the interior is reached (Aigner et al., 1996). The narrower sections of the heater will have a higher resistance, and thus the power generated, which is linear in the heater resistance for constant current, will be greater. This excess power can be designed to compensate for the thermal conduction losses on the outer portion of the device. In the case of Figure 6-7, the standard deviation in temperature was 8 °C. In Figure 6-8 a set of different microheater designs is compared for thermal uniformity (Lee et al., 2003). Improved reactivity and sensitivity was observed for the most design with the most uniform temperature profile (Figure d) due to the larger isothermal active area. By reducing hotspots, the device lifetime is also increased. The device in Figure d was shown to be stable for 1000 h at 500 °C. The increasing use of modulated temperature modes motivated the use of a time-resolved thermal imaging technique to show how thermal uniformity can change in time (Cavicchi et al., 2004). Figure 6-9 shows the initial heating and subsequent cooling from a 40 μ s pulse applied to the upper heater of the microcalorimeter shown in Figure 6-6. At short times, Figure 6-9 (a) and (b), the thermal distribution matches the shape of the upper heater. At 1.9 ms after the pulse, Figure 6-9 (c), the lower zone of the structure has warmed significantly, while at 3.9 ms, Figure 6-9 (d), the temperature has fully equilibrated across the device. Thermographic measurements have also revealed detailed information about materials issues that may affect sensor performance. For example, Furjes et al observed that drop deposited thick film sensing materials may contain voids that result in a much lower temperature on portions of the sensing material (Furjes et al., 2005) as shown in Figure 6-10. Thermal modeling can be used to design structures to optimize thermal uniformity and minimize power consumption (Kolev et al., 2000) (Kozlov, 2002a, Kozlov, 2002b, Lee et al., 2003).

Application of thick film sensing materials to a thin micromachined membrane can result in breakage and lower yield of devices. Ducso et al found that by stopping the micromachining etch to leave a small vertical pillar supporting the center of the membrane enhanced the mechanical stability of the device for deposition of a thick porous sensing film (Ducso et al., 2003). The mass of the sensing film was more than ten times the mass of the membrane itself. The vertical pillar, however, did increase the power consumption of the device relative to a fully etched device by approximately fifty percent.

A nanoscale “hotspot” calorimetric gas sensor device has been demonstrated that has very low power consumption (Kovalgin et al., 2006). The device takes advantage of a conductive link formed between two polysilicon layers separated by SiO₂. The link is formed by applying a high voltage that breaks down the oxide, resulting in a narrow, nanoscale channel of conduction between the two layers. In principal, other nanoscale calorimetric gas sensors should be possible using nanofabrication techniques, single

carbon nanotubes, or metallic nanowires.

4. Materials

The key element to the calorimetric gas sensor, is the material that interfaces with the gas. Catalytic sensors require a catalyst that efficiently promotes combustion of the target analyte. The activity of a catalyst varies with temperature. For example, for methane combustion, Pd works effectively at a lower temperature than Pt. The form of the catalyst, from thin film to nanoparticle dispersion, strongly affects activity and poison resistance (discussed in the following section.) Also of importance is the interaction with the support material. Calorimetric sensing that is based purely on physical effects such as the difference in the thermal conductivity between air and analyte or the detection of desorption are also sensitive to the choice of materials for the air/sensor interface.

For a catalytic sensor, using the MEMS platform, the simplest method is to use thin film deposition to produce a Pt or Pd film as the layer on the device to be exposed to the gas environment (Manginell et al., 1996, Hierlemann and Baltes, 2003, Cavicchi et al., 2004). This form of the device is analogous to the original catalytic wire sensors, for which it was found that improvement could be obtained through the use of nanotextured materials. Bartlett and Guerin reported the use of an electrochemical method to deposit nanotextured Pd (Bartlett and Guerin, 2003). The approach used a solution made from Pd-containing molecule ammonium tetrachloropalladate and the molecule octaethyleneglycol monohexadecyl ether, which formed a lyotropic liquid crystal. The deposition took place only on the gold electrode fabricated on the heater membrane and resulted in an effective surface area of in excess of $10^6 \text{ cm}^2/\text{cm}^3$. Compared to a film Pd film deposited from an aqueous solution which showed very little response to methane at 500°C , the nanotextured film had a linear response to concentrations up to 2.5 percent methane in air, with a sensitivity of a sensitivity of 35 mV/% methane, and exhibited stable performance for three hours. S. M. Lee et al (Lee et al., 2003) also more recently used this approach. J. S. Lee et al. used an annealing technique to convert a continuous bilayer of alumina and Pd into a nanoparticle supported catalyst (Lee et al., 1997). A common approach is to apply a drop coating of catalyst and oxide that is subsequently annealed (Katti et al., 2002, Krebs and Grisel, 1993, Ducso et al., 2003, Engel et al., 2004, Kulinyi et al., 2005) (Ducso et al., 2003, Furjes et al., 2005) or to use screen printing followed by annealing (Debeda et al., 1995, Han et al., 2007b). Houlet et al used a Pt-alumina paste on a MEMS device for hydrogen sensing (Houlet et al., 2008). Sometimes a two-step process is used, depositing a porous oxide first, and impregnating the oxide with Pt catalyst via a dropped on coating of platinumic acid (Aigner et al., 1996) or a solution containing PtCl_2 (Lv et al., 2007). Engel et al. used only PtCl_2 (Engel et al., 2004).

By using an array of sensors, the capability for chemical selectivity is enhanced. Different catalytic coatings have different chemical sensitivities. The information gleaned from multiple sensors can be analyzed to produce a desired chemical selectivity. An example is the use by Debeda et al. of a dual sensor (Debeda et al., 1995), (Debeda et al., 1997) one sensor with a Pd coating and a second with a Pt coating. At an operating

temperature of 400 °C, the Pd-coated sensor is sensitive to all combustible gases, while the Pt sensor detects most combustible gases except methane. By subtracting the results (after appropriate scaling), the concentration of methane can be determined.

The oxidation state of the catalyst can play an important role in the sensing process. In an x-ray photoemission spectroscopy (XPS) study of Pd catalyst supported on alumina, see Figure 6-11, Hoogers et al. (Hoogers et al., 1992) show that at 300 °C, the temperatures use for hydrogen sensing, the Pd is partially oxidized, and hydrogen can change the oxidation state, while at 500 °C, in the range of temperatures used for methane sensing, the Pd is fully oxidized, and hydrogen does not change the oxidation state.

Casey et al. report a catalytic sensor that operates at room temperature, using a polymer-supported Pt catalyst (Casey et al., 2003). The temperature rise is detected by a SnO₂/Al or SnO₂/Au thermopile. A hydrogen sensing calorimeter has been reported that uses TiO₂ nanotubes as the support for the Pd catalyst (Han et al., 2007b). Lower temperature operation of a TiO₂/Pd sensor was accomplished by using ultraviolet light to create oxygen species on the TiO₂ catalyst support (Han et al., 2007a).

Recently zeolites have been used as a support material with the idea of using the pore size to enhance the chemical selectivity (Yasuda et al., 2009). The zeolite materials activated with Pd by stirring with an ammonia/palladium(II) nitrate solution. Dried solids were mixed into slurry with water and dropped onto a micromachined sensor platform. Sensors made from zeolites with pores of average size 0.4 nm were selective to CO, while sensors pore size of 0.75 nm showed a similar response to CO, but also a response to N-hexane and cyclohexane.

In thermal conductivity sensors there is a heated element whose temperature will change if the thermal conductivity of the gas changes. Because hydrogen has a much higher thermal conductivity than air, this principle can be used to detect hydrogen for safety applications (Arndt, 2002). The physical sensing approach has also been used by combining a calorimetric platform with a polymer layer that can adsorb organic volatiles. A thermopile is used to detect the temperature changes caused by adsorption (Kerness et al., 2000).

5. Poisoning

One of the key factors affecting the life of calorimetric gas sensor sensors is the reduction of the catalyst activity due to contaminating gases in the environment. Gentry and Walsh performed comprehensive studies of the poisoning effects in pellistors (Gentry and Walsh, 1984, Gentry and Walsh, 1987). They compared three classes of contaminants, sulphur-containing, halogenated and high molecular weight species. Differences between catalysts and their methods of support and dispersion were studied. These classifications have served as the basis for subsequent work in this aspect of the technology.

Halogenated gases were found to reversibly inhibit catalytic activity by adsorbing on the catalyst and blocking sites for combustion. Sulphur-containing species often resulted in

partially irreversible changes that took longer to establish. Gentry and Walsh propose that a SO_2 species is formed through a reaction with the catalyst. When the poison is removed, partial recovery takes place through the desorption of SO_2 . For both halogenated and sulphur-containing species, when comparing three catalysts, both the gas sensitivity and susceptibility to poisoning were found to proceed as $\text{Pd} > \text{Rh} > \text{Pt}$. Deng et al compared Pd, Rh, and Ir catalysts in a study of sulphur poisoning (Deng et al., 1993). Ir, while less catalytically active for methane oxidation, was the least affected by SO_2 poisoning. An oscillatory response was observed on calorimetric gas sensors exposed to 10 ml/l methane and 0.2 ml/l SO_2 in air.

In industrial environments, silicon-containing gases can result in the poisoning of the catalyst. Hexamethyldisiloxane (HMDS) has been studied as a high molecular weight model contaminant (Gentry and Walsh, 1984, Gentry and Walsh, 1987, Ehrhardt et al., 1997). Gentry and Walsh reported that HDMS irreversibly poisons catalysts. The effect is reduced with increased porosity of the support and increased dispersion of the catalyst. In an early study of a MEMS methane sensor, Krebs et al. found that thick film catalysts to be more resistant to HDMS poisoning (Krebs and Grisel, 1993). XPS measurements of a Pt film exposed at 632 °C and 722 °C, as shown in Figure 6-12, showed the presence of Si, O, and increased C, with an accompanying decrease in Pt (Ehrhardt et al., 1997). The energy values of the Si 2s and O 1s peaks indicated the formation of a SiO_2 layer on the Pt, which inhibits the interaction between the combustible gas and the catalytic film. Continued operation of the Pt film in the absence of HMDS results in some recovery in the sensitivity of the Pt to the combustible gas, and also some reduction in the XPS signals assigned to SiO_2 . The authors suggest that the initial continuous overlayer of SiO_2 fragments into islands, which allows partial recovery of activity. Matsumiya et al. examined lower temperature exposures of Pt to HMDS with the view of H_2 sensing (Matsumiyaa et al., 2003). In these experiments, XPS also provided evidence of the formation of a SiO_2 layer. The rate of formation of this layer was greatly accelerated at 200 °C, compared to 100 °C. Annealing in vacuum at 400 °C of a poisoned surface provided partial recovery. Auger depth profiling suggested a mean thickness of 3 nm, for a 72 h exposure to 1 mmol/mol concentration of HDMS in air at 100 °C. It was found that the thin SiO_2 layer produced by HDMS exposure was actually useful in improving the selectivity of the hydrogen sensor. A similar utilization of HDMS exposure was exploited by Sommer et al. where a pair of sensors was used, one having been exposed to HDMS (Sommer et al., 1993). The sensitivity of the HDMS sensor to methane was greatly reduced compared to the sensitivity to butane.

Selection and size of the catalyst, and the porosity of the oxide support have been shown to affect the poison resistance of devices. It is also possible to add protective coatings. For example, a polytetrafluoroethylene coating was used to reduce poisoning due to HDMS, H_2S , and iodine for a hydrogen calorimetric gas sensor (Katti et al., 2002), while Miller reports the use of an alumina coating (Miller, 2001).

6. Signal Analysis and Operating Modes

While a conventional calorimetric gas sensor operating at a fixed temperature is a very

useful device for determining if a combustible gas is present, for many applications it is desirable to identify the gas species responsible for combustion. The ability to analyze mixtures is also desirable. One of the simplest methods for obtaining chemical selectivity from this technology is to use an array of sensors operating at different fixed temperatures and make use of the difference in the onset temperature of combustion for different gases. An example of this method is the work of Riegel and Hardtl (Riegel and Haerdtl, 1990), where a set of eight BaTiO₃ thermistors with a catalyst coating was used. Each thermistor was tuned to have a very sensitive temperature coefficient of resistivity at a different working temperature. Figure 6-13 shows an example of the results obtained for hydrogen, CO, ethanol, propane, and butane with different thresholds for combustion for the different gases.

Rose and Zdanevitch demonstrated the use of time-varying temperature programs to operate a Pt wire calorimeter (Rose and Zdanevitch, 1995). A parameter was developed that distinguishes between gases based on the difference between the temperature of the onset of combustion and the temperature at which combustion saturates. It was found that this parameter was sufficient to identify hydrogen, alcohol, methane, butane, and propane. Using a commercially available pellistor, Bandomir et al. used a triangle ramp of 600 s duration applied to the heater to produce a dataset that was analyzed by an artificial neural network (Bandomir et al., 2005). It was found that it was possible to separate hydrogen from other hydrocarbons, but the separations between hydrocarbons were not sufficient to distinguish hydrocarbons using a single sensor.

Gall showed that with a MEMS device three methods signal enhancement were possible (Gall, 1993). Figure 6-14 shows results he obtained for different gases as a function of inverse temperature. These results were used to define the operating temperature for an array of sensors with identical Pt catalyst set to different temperatures. The tested gases were methanol, ethanol, pentane, trichloroethylene, carbon monoxide, and methane. The results were analyzed with a neural network. All test gases were separated, although the results were only barely resolved for methanol and ethanol (as expected given the similarity of results for those two gases in Figure 6-14.) The second method of enhancement was to utilize different catalysts in the array. By using an additional Ir-coated sensor in the array, it was possible to achieve a larger separation between methanol and ethanol. The third method was to vary temperature as a function of time on a single device. Using this technique, Gall was able to separately identify four different alcohol vapors. Niebling et al. (Niebling et al., 1996) obtained similar results

With a MEMS device, Engel et al. used stepped temperature operation of a calorimeter was to distinguish between gasoline and diesel fuels (Engel et al., 2004). In this work, linear discriminant analysis combined was used to select the temperatures that produced the greatest information content for discrimination, these temperatures were then used in an artificial neural network to provide discrimination in one cycle (2 s) of data. In a different approach, sinusoidal modulation of the temperature can be obtained using a feedback network to control the delivered power to a microheater heater (Aigner et al., 1996) (Niebling et al., 1996). The sinusoidal modulation of temperature is imposed in addition to a gradual sweep in temperature by a steadily increasing unmodulated

component to the power. In the absence of a combustible gas, the modulated power will be sinusoidal, while in the presence of the combustible gas, the power will deviate strongly from sinusoidal near the onset of catalytic reactions on the sensor surface. This will generate harmonics that can be measured as the average temperature is swept from the minimum to maximum. Different combustible gases, will in general have different onset temperatures as in Figures 6-13 and 6-14, thus leading to differences in the harmonics as shown in Figure 6-15. These signals can be distinguished by pattern recognition techniques.

Using the device shown in Figure 6-6, Cavicchi et al. applied a periodic temperature ramp to both sides of the calorimeter (Cavicchi et al., 2004). The ramps to each side were adjusted so that only in the presence of analyte would the thermopile produce a voltage. Because of the different properties of the gases as they interact with the Pd surface, both for combustion and through desorption, response profiles were developed that could be used as fingerprints to identify the analytes as shown in Figure 6-16.

Without added catalysts, the calorimetric gas sensor device can act as a thermal conductivity sensor. By combining both thermal conductivity sensors with combustion (catalytic) sensors in an array, enhanced chemical selectivity can be achieved through the analysis of the array response (Ducso et al., 2003).

7. Packaging

Use of a flow through design, as shown in Figure 6-17 reduces the time required for gas to diffuse to the sensor head (Dabill et al., 1987). A response time of 1 s was reported. Kulinyi showed how reduction of the power consumption of the sensors, in addition to a polling method for interrogating sensors in an array could reduce the power consumption of electronics so that only explosion proof containment is needed for the sensor and not the electronics (Kulinyi et al., 2005). Norman et al. examined the effect of packaging on the performance of a microfabricated calorimetric gas sensor with the goal of producing a low power explosion proof device (Norman et al., 2003). They implemented a diffuser and a filter into a standard TO package as shown in Figure 6-18 (a). The purpose of the diffuser is explosion proofing, while the filter is to remove potential species that might poison the catalyst. Effects of some filter types have been described by Walsh (Walsh and Jones, 1991) and the benefits of a carbon filter to prevent HDMS poisoning was shown by Miller (Miller, 2001). Figure 6-18 (b) shows the response of a sensor exposed at time 1 minute to a concentration of propane in air equal to two percent of the LEL (Norman et al., 2003). The sensor is based on a Co_3O_4 coated microheater operating at 400 °C for three cases of packaging: no filter and no diffuser, no filter, and filter with diffuser. The impact of these on the response time and signal amplitude is evident, and shows the importance of considering the packaging in assessing the potential of new devices.

8. Applications

8.1 Gas detection

Table 2 provides a summary of some of the gases of interest and technologies and materials that have been reported for calorimetric gas sensors.

The most important application for calorimetric gas sensors continues to be in the area of safety. Situations where the ability to detect combustible gases is critical to safety include mines, transportation and processing of oil and gas, fuel type discrimination (Engel et al., 2004), leak detection in automotive fuel and exhaust systems, sewer gas and landfill gas. There are now a broader range of technologies available that calorimetric sensors must compete with (Hall, 2008) which acts to stimulate continued improvements in catalytic sensor technology.

Responses of calorimetric gas sensor to the variable conditions that might be found in a mine must be considered as part of the implementation of the technology. These include changes ambient pressure, oxygen concentration, and humidity. To use calorimetric gas sensor data to analyze an explosion based on recorded calorimetric gas sensor data will require knowledge of the effects of combustion products, large pressure variations, and the effects of particulates on the particular sensor (Willett et al., 1993).

An interesting example of a safety application is the detection of oxygen contamination in an atmosphere of hydrogen. This is the reverse of the traditional combustible gas-sensing situation! Because of its high thermal conductivity, hydrogen is used as a cooling agent in electric generators. In these applications, the risk of explosion is due to oxygen contamination of the system, so rather than probing the lower explosive limit, it is the upper explosive limit that the sensor must detect. The conventional method of detection of contaminants is through a thermal conductivity measurement. Quantitative measurements are problematic when contaminants of different thermal conductivities may be present. Use of calorimetric gas sensors has been explored for this application (Krawczyk and Namiesnik, 2003) and it was found that calorimetric gas sensor devices have a higher sensitivity, directly probe combustion, and can serve as an additional sensor that provides complementary information.

As mentioned earlier, calorimetric sensors based on thermal conductivity, rather than chemical reactivity, may find applications in hydrogen detection for fuel cells (Fawcett et al., 2006, Tardy et al., 2004, Simon and Arndt, 2002).

The ability of the new generation of MEMS devices to use arrays, rapid temperature modulation, and neural network analysis to achieve a chemically selective detection is opening up new applications. A MEMS calorimetric gas sensor operated in a temperature programmed mode was found to provide superior stability for discrimination between gasoline and diesel fuels, compared to semiconducting gas sensors (Engel et al., 2004). With lower detection limits and improved chemical selectivity, there is the potential of the devices to be useful for the monitoring of chemical processes and the monitoring of volatile organic compounds.

8.2 Biological Applications

While calorimetry has long been a useful tool in the biological and chemical sciences, there is a growing drive to produce miniaturized versions of the measurements. These devices can provide the benefits of small sample utilization, faster analysis, and parallel high-throughput data acquisition using arrays. An example application area is drug discovery. Calorimetric techniques may be divided into fixed and scanned temperature measurements. Fixed temperature measurements test for the thermal signal associated with a binding event or the energy change from an enzymatic reaction. These can be used in screening candidate drugs for reactions with target molecules. Scanned temperature measurements, such as Differential Scanning Calorimetry (DSC) and Differential Thermal Analysis (DTA) look for signals associated with a temperature dependent reaction, phase change, aggregation event, etc. Drug formulation stability is one of the applications of scanned temperature analysis. Conventional instruments require typically thirty minutes to perform a single scan. To achieve high-throughput screening of thousands of samples per day, a shift from a serial measurement to a parallel measurement paradigm is needed. Nanocalorimeter arrays (nano in terms not of nanometer scale, but nanojoule sensitivity or sometimes nanoliter volumes) are receiving increased attention.

The application of fixed and scanned temperature operating modes is closely analogous to operating modes used for calorimetric gas detection. The chief difference is that for biological applications, the temperature and temperature range is much lower, typically from 20 °C to 100 °C. Both thermopile and thermistor-based temperature measurement are used. Some examples of device applications, technology, and detection limits are shown in Table 3. With biological samples, there is the additional challenge of temperature noise in the presence of a liquid sample coming from convection and evaporation. A group at the Scripps-PARC Institute for Advanced Biomedical Sciences in Palo Alto, CA has also developed a 96 element in which an electrical pulse is used to drive two reacting drops together to start a reaction (Torres et al., 2004). Convection is reduced by having the two reactants close together on the same substrate and therefore at the same temperature prior to mixing. More recently the same group has replaced the Si based thermopile (used in the 2004 study) with a VO_x thermistor to achieve an eightfold temperature sensitivity improvement to 10 μK (Recht et al., 2008, Recht et al., 2009). Evaporation of the drop (and changed evaporation rates when the drops fuse), mixing, and baseline drift were the dominant factors contributing to the energy noise limit of 4.7J/l. Evaporation can be overcome using a design with a microfluidic channel (Lerchner et al., 2006). A temperature-scanned device has been used to measure the denaturation of the protein lysozyme (Wang et al., 2008).

9. Safety

The application of combustible gas detectors is usually motivated by safety considerations. When the technology is used to protect lives, it is important that hazardous gas detection is highly reliable. False alarms, such as can occur with sensors that respond to environmental changes that do not involve a combustible gas, or from

undesirable drift or failure of the sensor, can result in decreased confidence in the detection system. Failure to detect the presence of a combustible gas, as can occur when a sensor catalyst is poisoned, is an even worse possibility. The International Safety Equipment Association has published a procedure that recommends daily 'bump testing' of gas sensors to verify that the sensor is still functioning (ISEA, 2002). Failure of a bump test requires a full calibration. Under certain conditions, less frequent calibration is acceptable but a minimum of a thirty-day interval is specified. In the United States, these recommendations have been expanded under an Occupational Health and Safety Administration memo, which also specifies that calibration gas used to test a sensor be traceable to the National Institute of Standards and Technology (OSHA, 2004). The requirements for combustible gas detection devices have been published by various world standards organizations (IEC, 1999, ISAS, 2003, UL, 2004). The siting of sensors is critical to their effectiveness (DeFriend et al., 2008) and the development of realistic test conditions is important in realizing the desired performance of combustible gas sensors (Salyk et al., 2006).

10. Conclusions

The calorimetric combustible gas sensor has a long history of successful performance, with a demonstrated reliability for important safety applications. The competition from new, smaller infrared detectors is pushing the technology towards higher performance micromachined devices. Capabilities for enhanced chemical selectivity based on the use of arrays of micromachined sensors and/or fast temperature modulation have been demonstrated. Much lower power consumption makes possible applications where distributed battery-powered sensor nodes would be desirable. These devices, however, have yet to make a significant impact on the gas sensor market, with reliability and long term, reduced drift operation yet to be clearly demonstrated. Now that many interesting and promising capabilities have been demonstrated, there needs to be further research on how new nanomaterials can be integrated into the micromachined platforms to produce devices that can operate with lifetimes comparable or superior to the traditional catalytic bead device. Novel biosensor applications using the same MEMS technology are also promising.

	Calorimetric Sensor	Infrared Sensor	Semiconductor
Gases detected	All combustible gases	Depends on wavelength range of the unit, some gases, i.e. H ₂ , acetylene, CO, often not detected	Reducing gases, most combustible gases, but also non-combustible gases
Response time	10 s to 15 s	5 s to 10 s	10 s to 30 s
Sensitivity	~1000 µmol/mol	~1000 µmol/mol	~10 µmol/mol
Lifetime	5 years, but reduced depending on gas exposure	10 years	5 years, but reduced depending on gas exposure
Contamination	Certain gases can poison sensor, may lose sensitivity without warning	Condensation, fouling of optical surfaces. Use of a second beam provides a warning	Certain gases can poison sensor, may lose sensitivity without warning
Maintenance	Requires periodic gas testing	Less frequent, only for cleaning	Requires periodic gas testing
Cost for sensor system and servicing	Low	Higher than for calorimetric device	Lowest

Table 1. Comparison of gas sensing technologies for combustible gas detection.

Gas	Threshold Sensitivity	Technology	Temperature	Sensing Material	Reference
Ethanol, Methanol, Isopropanol	50-100 $\mu\text{mol/mol}$	Micromachined, with temperature modulation	480 °C, 65 mW	Pt-impregnated Al_2O_3	(Aigner et al., 1996)
Methanol, Ethanol, Benzene, Acetone, H_2	3 $\mu\text{mol/mol}$	Micromachined, thermopile with temperature modulation	20 °C-500 °C	Pd	(Cavicchi et al., 2004)
Propane, Butane	<3 mmol/mol	Micromachined	38 °C	Pt, Pd supported on Al_2O_3 or TiO_2	(Ducso et al., 2003)
Butane, Ethanol, Propane, CO , H_2	<1 mmol/mol for H_2 40 $\mu\text{mol/mol}$	BaTiO_3 thermistor	75 °C -320 °C	Pt	(Riegel and Haerdtl, 1990)
Butane, Ethanol, Methane, H_2	5 mmol/mol	Micromachined	400 °C	Pd thin film, Pd 'thick film catalyst'	(Krebs and Grisel, 1993)
Methane, Isobutane	<1 mmol/mol	Micromachined	350 °C	Pt/ Al_2O_3	(Lee et al., 1997)
Methane, Ethane	1 mmol/mol	Films on Al_2O_3 substrate	341 °C	Pd/ Al_2O_3	(Luo et al., 1991)
Methane	1.2 mmol/mol	Micromachined	500 °C	Electrochemically deposited nanostructured Pd	(Bartlett and Guerin, 2003)
Methane	7 mmol/mol	Thick film, dual sensor	400 °C	Pd for all combustibles, Pt for all except methane	(Debeda et al., 1997)
CO , N-hexane, cyclohexane	100 $\mu\text{mol/mol}$	Micromachined	295 °C	Pd-activated zeolite with varying pore size	(Yasuda et al., 2009)
H_2 and CO	30 $\mu\text{mol/mol}$	SnO_2 Thermopile	< 35 °C	Pt for H_2 , Pt/Ir for CO ; catalyst supported on polydivinylbenzene	(Casey et al., 2003)
CO , H_2	6 mmol/mol	Films on Al_2O_3 substrate	277 °C	Pd/Au	(Makovos et al., 1993)
Propylene, H_2	8	Micromachined	360 °C	Pd	(Zanini et al., 1995)

	$\mu\text{mol/mol}$				
H ₂	0.5 mmol/mol	Thermoelectric NiO thick film	100 °C	Pt thin film	(Shin et al., 2003)
H ₂	0.1 mmol/mol	Micromachined SiC, thermal conductivity	400 °C		(Fawcett et al., 2006)
H ₂	<1 mmol/mol	Cu/Bi thermopile on SU-8	65 °C	Pd	(Park et al., 2009)
H ₂	5 mmol/mol	Thick film with UV irradiation	82 °C	Pd/Pt supported on TiO ₂	(Han et al., 2007a)
H ₂	1 $\mu\text{mol/mol}$	Micromachined thermocouple	200 °C	Pt supported on Al ₂ O ₃	(Houlet et al., 2008)
H ₂	1 mmol/mol	Catalytic Bead	200 °C	Pd/Thoria on Al ₂ O ₃	(Jones and Nevell, 1989)
H ₂	10 mmol/mol	Glass coated Pt wire around Al ₂ O ₃ substrate	120°C	Pd supported on Al ₂ O ₃ with polymer poison resistant coating	(Katti et al., 2002)
H ₂	1.0 mmol/mol	Thermal conductivity	100 °C		(Arndt, 2002)

Table 2. Examples of combustible gases detected for different calorimetric technologies, operating temperatures, and sensing materials.

Application	Volume (μl)	Min detected Power (nW)	Thermometer	Temperature Noise (μK)	Sensitivity V/W	Minimum Detected Energy (μJ)	Reference
Enzyme Reactions	20	50 in water (8 in air)	Thermopile: 118 junction BiSb/Bi	100 (in liquid) 20 (dry)	4	4	(Lerchner et al., 2006)
Protein ligand: streptavidin biotin Enzyme Reactions: hexokinase +1 mM glucose Organelle: Mitochondria +DNP ITC	0.50	10 (in air) 500 (in water)	Thermistor: Amorphous Si and VOx	80 (amorphous Si) 10 (VOx)		2	(Torres et al., 2004) (Recht et al., 2008, Recht et al., 2009)
Enzyme Reactions:	0.0007	10	Thermopile: 10 junction	125	2.5		(Johannesse n et al.,

bovinelivercatalase/H ₂ O ₂ Single Cell: mouse liver ITC			Ni/Au				2002)
Cells ITC	10	50	Thermopile	50	23	3	(Verhaegen et al., 1999)
Enzyme reactions: glucose oxidase creatinine deiminase ITC	10		Thermopile: 120 junction Si/Al	20	8(in air) 3.6(in water) 1.3(with flow)		(Vanherwaarden et al., 1994)
Enzyme reactions: urea-urease, glucose oxidase bovinelivercatalase/ H ₂ O ₂	0.015	50	Thermopile: 16 junction Au/Si	30	1V/W		(Zhang and Tadigadapa, 2004)
DSC Denaturation of lysozyme	1	50	Thermopile: 30 junction Ni/Cr	21	.78		(Wang et al., 2008)
Hexadecanethiol on Au DSC	.035	3/0.7	Pt film	13000			(Zhang et al., 2004)
ascorbic acid, ascorbate oxidase ITC	10		Thermopile: 26 junction Cr/Cu	7000			(Kwak et al., 2008)
DSC Denaturation of Glucose Oxidase	0.1	130	Thermistor: Ge	100			(Weiss et al., 2007)

Table 3. Applications of microcalorimeters for biological applications.

References

- Aigner, R., Dietl, M., Katterloher, R. & Klee, V. (1996) Si-planar-pellistor: Designs for temperature modulated operation. *Sens Actuators B Chem*, 33, 151-155.
- Arndt, M. (2002) Micromachined thermal conductivity hydrogen detector for automotive applications. *Sensors*, 2002. Orlando, FL.
- Baker, A. R. (1962) Gb892530 (a). U.K., National Research Development Corporation.
- Bandomir, R., Krawczyk, M. & Namiesnik, J. (2005) A new analyzer based on pellistor sensor with neural network data postprocessing for measurement of hydrocarbons in lower explosive limit range. *J Autom Methods Manag Chem*, 2, 55-57.
- Bársony, I., Dücső, C. & Fürjes, P. (2009) Thermometric gas sensing. IN Comini, E., Faglia, G. & Sberveglieri, G. (Eds.) *Solid state gas sensing*. Heidelberg, Springer.
- Bartlett, P. N. & Guerin, S. (2003) A micromachined calorimetric gas sensor: An application of electrodeposited nanostructured palladium for the detection of combustible gases. *Anal Chem*, 75, 126-132.
- Casey, V., Cleary, J., D'arcy, G. & Mcmonagle, J. B. (2003) Calorimetric combustible gas sensor based on a planar thermopile array: Fabrication, characterisation, and gas response. *Sens Actuators B Chem*, 96, 114-123.
- Cavicchi, R. E., Poirier, G. E., Tea, N. H., Afridi, M., Berning, D., Hefner, A., Suehle, J., Gaitan, M., Semancik, S. & Montgomery, C. (2004) Micro-differential scanning calorimeter for combustible gas sensing. *Sens Actuators B Chem*, 97, 22-30.
- Dabill, D. W., Gentry, S. J. & Walsh, P. T. (1987) A fast-response catalytic sensor for flammable gases. *Sens Actuators*, 11, 135-143.
- Debeda, H., Dulaua, L., Dondona, P., Menila, F., Lucata, C. & Massokb, P. (1997) Development of a reliable methane detector. *Sens Actuators B Chem*, 248-256.
- Debeda, H., Rebiere, D., Pistre, J. & Menil, F. (1995) Thick-film pellistor array with a neural-network posttreatment. *Sens Actuators B Chem*, 27, 297-300.
- Defriend, S., Dejmek, M., Porter, L., Deshotels, B. & Natvig, B. (2008) A risk-based approach to flammable gas detector spacing. *J Hazard Mater*, 159, 142-151.
- Deng, Y. Q., Nevell, T. G., Ewen, R. J., Honeybourne, C. L. & Jones, M. G. (1993) Sulfur poisoning, recovery and related phenomena over supported palladium, rhodium and iridium catalysts for methane oxidation. *Appl Catal A Gen*, 101, 51-62.
- Ducso, C., Adam, M., Furjes, P., Hirschfelder, M., Kulinyi, S. & Barsony, I. (2003) Explosion-proof monitoring of hydrocarbons by mechanically stabilised, integrable calorimetric microsensors. *Sens Actuators B Chem*, 95, 189-194.
- Ehrhardt, J. J., Colin, L. & Jamois, D. (1997) Poisoning of platinum surfaces by hexamethyldisiloxane (hmds) : Application to catalytic methane sensors. *Sens Actuators B Chem*, 117.
- Engel, M., Baumbach, M., Kammerer, T. & Schutze, A. (2004) Preparation of microstructured pellistors and their application for fast fuel vapor

- discrimination. *17th IEEE International Conference on MEMS*. Maastricht, The Netherlands.
- Fawcett, T. J., Wolan, J. T., Spetz, A. L., Reyes, M. & Sadow, S. E. (2006) Thermal detection mechanism of sic based hydrogen resistive gas sensors. *Appl Phys Lett*, 89.
- Firth, J. G., Jones, A. & Jones, T. A. (1973) The principles of the detection of flammable atmospheres by catalytic devices. *Combust Flame*, 21, 301-311.
- Frost and Sullivan, (2006) World industrial gas sensors detectors and analyzers markets. MC1377591
- Furjes, P., Adam, M., Ducso, C., Zettner, J. & Barsony, I. (2005) Thermal effects by the sensitive coating of calorimetric gas sensors. *Sens Actuators B Chem*, 111, 96-101.
- Furjes, P., Vizvary, Z., Adam, M., Barsony, I., Morrissey, A. & Ducso, C. (2002a) Materials and processing for realization of micro-hotplates operated at elevated temperature.
- Furjes, P., Vizvary, Z., Adam, M., Morrissey, A., Ducso, C. & Barsony, I. (2002b) Thermal investigation of micro-filament heaters. *Sens Actuators A Phys*, 99, 98-103.
- Gall, M. (1991) The si planar pellistor - a low-power pellistor sensor in si thin-film technology. *Sens Actuators B Chem*, 4, 533-538.
- Gall, M. (1993) The si-planar-pellistor array, a detection unit for combustible gases. *Sens Actuators B Chem*, 16, 260-264.
- Gentry, S. J. & Walsh, P. T. (1984) Poison-resistant catalytic flammable-gas sensing elements. *Sens Actuators*, 5, 239.
- Gentry, S. J. & Walsh, P. T. (1987) The theory of poisoning of catalytic flammable gas-sensing elements. IN Moseley, P. T. & Tofield, B. C. (Eds.) *Solid state gas sensors*. Bristol and Philadelphia, Adam Hilger.
- Hall, B. (2008) Workplace safety for hazardous areas—minimizing risks by using gas detection. *Hazardous Areas Conference 2008 – IDC Technologies*. Johannesburg, South Africa, IDC Technologies.
- Han, C. H., Hong, D. W., Han, S. D., Gwak, J. & Singh, K. C. (2007a) Catalytic combustion type hydrogen gas sensor using tio₂ and uv-led. *Sens Actuators B Chem*, 125, 224-228.
- Han, C. H., Hong, D. W., Kim, I. J., Gwak, J., Han, S. D. & Singh, K. C. (2007b) Synthesis of pd or pt/titanate nanotube and its application to catalytic type hydrogen gas sensor. *Sens Actuators B Chem*, 128, 320-325.
- Hierlemann, A. & Baltes, H. (2003) Cmos-based chemical microsensors. *Analyst*, 128, 15 - 28.
- Hoogers, G., Huck, R., Kohl, D. & Heiland, G. (1992) The uptake of oxygen by noble-metal clusters on gas sensors. *Sens Actuators B Chem*, 9, 123-125.
- Houlet, L. F., Shin, W., Tajima, K., Nishibori, M., Izu, N., Roh, T. & Matsubara, I. (2008) Thermopile sensor-devices for the catalytic detection of hydrogen gas. *Sens Actuators B Chem*, 130, 200-206.
- International Electrotechnical Commission, (1999) Guide for the selection, installation, use and maintenance of apparatus for the detection and measurement of flammable gases International Standard IEC 61779-6

- The Instrumentation, Systems, and Automation Society, American National Standards Institute, (2003) Performance requirements for combustible gas detectors. ANSI/ISA 12.13.01-2003
- Isea (2002) Isea statement on verification of calibration for. Direct reading portable gas monitors used in confined spaces. International Safety Equipment Association.
- Johannessen, E. A., Weaver, J. M. R., Cobbold, P. H. & Cooper, J. M. (2002) Heat conduction nanocalorimeter for pl-scale single cell measurements. *Appl Phys Lett*, 80, 2029-2031.
- Jones, E. (1987) The pellistor gas catalytic gas detector. IN Moseley, P. T. & Tofield, B. C. (Eds.) *Solid state gas sensors*. Bristol and Philadelphia, Adam Hilger.
- Jones, M. G. & Nevell, T. G. (1989) The detection of hydrogen using catalytic flammable-gas sensors. *Sens Actuators*, 16, 215-224.
- Katti, V. R., Debnath, A. K., Gadkari, S. C., Gupta, S. K. & Sahni, V. C. (2002) Passivated thick film catalytic type h-2 sensor operating at low temperature. *Sens Actuators B Chem*, 84, 219-225.
- Kerness, N., Koll, A., Schaufelbuehl, A., Hagleitner, C., Hierlemann, A., Brand, O. & Baltes, H. (2000) N-well-based cmos calorimetric chemical sensors. *IEEE Workshop MEMS 2000*. Miyazaki, Japan.
- Kolev, S. D., Adam, M., Ducso, C., Barsony, I., Cobianu, C. & Van Den Berg, A. (2000) Thermal modelling of a porous silicon-based pellistor-type catalytic flammable gas sensor with two supporting beams. *Microelectronics J*, 31, 339-342.
- Kovalgin, A. Y., Holleman, J., Iordache, G., Jenneboer, T., Falke, F., Zieren, V. & Goossens, M. J. (2006) Low-power, antifuse-based silicon chemical sensor on a suspended membrane. *J Electrochem Soc*, 153, H181-H188.
- Kozlov, A. G. (2002a) Analytical modelling of steady-state temperature distribution in thermal microsensors using fourier method part 2. Practical application. *Sens Actuators A Phys*, 101, 299-310.
- Kozlov, A. G. (2002b) Optimization of structure and power supply conditions of catalytic gas sensor. *Sens Actuators B Chem*, 82, 24-33.
- Krawczyk, M. & Namiesnik, J. (2003) Application of a catalytic combustion sensor (pellistor) for the monitoring of the explosiveness of a hydrogen-air mixture in the upper explosive limit range. *J Autom Methods Manag Chem*, 25, 115-122.
- Krebs, P. & Grisel, A. (1993) A low-power integrated catalytic gas sensor. *Sens Actuators B Chem*, 13, 155-158.
- Kulinyi, S., Brandszajsz, D., Amine, H., Adam, M., Furjes, P., Barsony, I. & Ducso, C. (2005) Olfactory detection of methane, propane, butane and hexane using conventional transmitter norms. *Sens Actuators B Chem*, 111, 286-292.
- Kwak, B. S., Kim, B. S., Cho, H. H., Park, J. S. & Jung, H. I. (2008) Dual thermopile integrated microfluidic calorimeter for biochemical thermodynamics. *Microfluid Nanofluid*, 5, 255-262.
- Lee, J. S., Park, J. W. & Shin, S. M. (1997) Fabrication of a micro catalytic gas sensor using thin film process and si anisotropic etching techniques. *Sens Actuators B Chem*, 45, 265-269.

- Lee, S. M., Dyer, D. C. & Gardner, J. W. (2003) Design and optimisation of a high-temperature silicon micro-hotplate for nanoporous palladium pellistors. *Microelectronics J*, 34, 115-126.
- Lerchner, J., Wolf, A., Wolf, G., Baier, V., Kessler, E., Nietzsche, M. & Krugel, M. (2006) A new micro-fluid chip calorimeter for biochemical applications. *Thermochim Acta*, 445, 144-150.
- Luo, R. X., Chen, L. H., Chen, A. F. & Liu, C. C. (1991) A novel catalytic sensor for monitoring the concentration of mixed combustible gases. *Sci China Ser A-Math Phys Astron.*, 34, 1500-1507.
- Lu, X. Q., Zhang, Z. Y. & Kong, D. Y. (2007) A catalytic sensor using mems process for methane detection in mines. *Proceedings of the 2007 International Conference on Information Acquisition*. Jeju City, Korea.
- Makovos, E. B., Montague, F. W., Dudik, L. & Liu, C. C. (1993) A calorimetric combustible gas detector employing platinum film heaters. *Sens Actuators B Chem*, 12, 91-94.
- Manginell, R. P., Smith, J. H., Ricco, A. J., Moreno, D. J., Hughes, R. C., Huber, R. J. & Senturia, S. D. (1996) Selective, pulsed cvd of platinum on microfilament gas sensors. *Solid State Sensor and Actuator Workshop*. Hilton Head, SC.
- Matsumiyaa, M., Shin, W., Qiu, F., Izua, N., Matsubaraa, I. & Murayamaa, N. (2003) Poisoning of platinum thin film catalyst by hexamethyldisiloxane (hmde) for thermoelectric hydrogen gas sensor. *Sens Actuators B Chem*, 96, 516-522.
- Miller, J. B. (2001) Catalytic sensors for monitoring explosive atmospheres. *IEEE Sens J*, 1, 88.
- Niebling, G., Aigner, R., Wabner, D. & Menzel, R. (1996) Data reduction for curve analysis. *Sens Actuators B Chem*, 34, 481-486.
- Norman, A., Stam, F., Morrissey, A., Hirschfelder, M. & Enderlein, D. (2003) Packaging effects of a novel explosion-proof gas sensor. *Sens Actuators B Chem*, 95, 287-290.
- Occupational Safety and Health Administration, (2004) Verification of calibration for direct-reading portable gas monitors. Safety Health Information Bulletin SHIB 05-04-2004.
- Park, S. C., Yoon, S. I., Lee, C. I., Kim, Y. J. & Song, S. H. (2009) A micro-thermoelectric gas sensor for detection of hydrogen and atomic oxygen. *Analyst*, 134, 236-242.
- Recht, M. I., De Bruyker, D., Bell, A. G., Wolkin, M. V., Peeters, E., Anderson, G. B., Kolatkar, A. R., Bern, M. W., Kuhn, P., Bruce, R. H. & Torres, F. E. (2008) Enthalpy array analysis of enzymatic and binding reactions. *Anal Biochem*, 377, 33-39.
- Recht, M. I., Torres, F. E., De Bruyker, D., Bell, A. G., Klumpp, M. & Bruce, R. H. (2009) Measurement of enzyme kinetics and inhibitor constants using enthalpy arrays. *Anal Biochem*, 388, 204-212.
- Riegel, J. & Haerdtl, K. H. (1990) Analysis of combustible gases in air with calorimetric gas sensors based on semiconducting batio₃ ceramics. *Sens Actuators B Chem*, 1, 54-57.

- Rose, G. & Zdanevitch, I. (1995) A new method using a catalytic sensor for the identification and concentration measurement of combustible gases. *Sens Actuators B Chem*, 25, 426-428.
- Salyk, O., Castello, P. & Harskamp, F. (2006) A facility for characterization and testing of hydrogen sensors. *Meas Sci Technol*, 17, 3033-3041.
- Shin, W., Matsumiya, M., Izu, N. & Murayama, N. (2003) Hydrogen-selective thermoelectric gas sensor. *Sens Actuators B Chem*, 93, 304-308.
- Simon, I. & Arndt, M. (2002) Thermal and gas-sensing properties of a micromachined thermal conductivity sensor for the detection of hydrogen in automotive applications. *Sens Actuators A Phys*, 97-8, 104-108.
- Sommer, V., Tobias, P. & Kohl, D. (1993) Methane and butane concentrations in a mixture with air determined by microcalorimetric sensors and neural networks. *Sens Actuators B Chem*, 12, 147-152.
- Tardy, P., Coulon, J. R., Lucat, C. & Menil, F. (2004) Dynamic thermal conductivity sensor for gas detection. *Sens Actuators B Chem*, 98, 63-68.
- Torres, F. E., Kuhnt, P., De Bruyker, D., Bell, A. G., Wolkin, M. V., Peeters, E., Williamson, J. R., Anderson, G. B., Schmitz, G. P., Recht, M. I., Schweizer, S., Scott, L. G., Ho, J. H., Elrod, S. A., Schultz, P. G., Lerner, R. A. & Bruce, R. H. (2004) Enthalpy arrays. *Proc Natl Acad Sci USA*, 101, 9517-9522.
- Underwriters Laboratories, (2004) Standard for gas and vapor detectors and sensors. NSI/UL 2075
- Vanherwaarden, A. W., Sarro, P. M., Gardner, J. W. & Bataillard, P. (1994) Liquid and gas micro-calorimeters for (bio)chemical measurements. *Sens Actuator A-Phys*, 43, 24-30.
- Verhaegen, K., Baert, K., Puers, B., Sansen, W., Simaels, J., Driessche, W. V. & Hermans, L. (1999) A silicon microphysiometer for high-throughput drug screening. *Micro- and nanofabricated structures and devices for biomedical environmental applications*. San Jose CA, Society of Photo-Optical Instrumentation Engineers.
- Walsh, P. & Jones, T. A. (1991) Calorimetric chemical sensors. IN Gopel, W., Hesse, J. & Zemel, J. N. (Eds.) *Sensors - a comprehensive survey*. Weinheim, VCH.
- Wang, L., Sipe, D. M., Xu, Y. & Lin, Q. (2008) A mems thermal biosensor for metabolic monitoring applications. *J Microelectromech Syst*, 17, 318-327.
- Weiss, T., Igel, G. & Urban, G. (2007) Chip-based scanning nano-calorimeter for protein stability analysis in biosensor membranes. *Solid-State Sensors, Actuators and Microsystems Conference, 2007. TRANSDUCERS 2007. International*. Lyon, France, IEEE.
- Willett, M. J., Wykes, J. S. & Gibson, M. J. (1993) The behavior of catalytic methanometers in simulated explosion conditions. *Sens Actuators B Chem*, 12, 181-193.
- Yasuda, K. E., Visser, J. H. & Bein, T. (2009) Molecular sieve catalysts on microcalorimeter chips for selective chemical sensing. *Microporous Mesoporous Mater*, 119, 356-359.
- Zanini, M., Visser, J. H., Rimai, L., Soltis, R. E., Kovalchuk, A., Hoffman, D. W., Logothetis, E. M., Bonne, U., Brewer, L., Bynum, O. W. & Richard, M. A.

- (1995) Fabrication and properties of a si-based high-sensitivity microcalorimetric gas sensor. *Sens Actuators A Phys*, 48, 187-192.
- Zhang, Y. Y. & Tadigadapa, S. (2004) Calorimetric biosensors with integrated microfluidic channels. *Biosens Bioelectron*, 19, 1733-1743.
- Zhang, Z. S., Wilson, O. M., Efremov, M. Y., Olson, E. A., Braun, P. V., Senaratne, W., Ober, C. K., Zhang, M. & Allen, L. H. (2004) Heat capacity measurements of two-dimensional self-assembled hexadecanethiol monolayers on polycrystalline gold. *Appl Phys Lett*, 84, 5198-5200.

Figure Captions

Figure 6-1. Cutaway illustration of a conventional pellistor device, showing the Pt heater wire and surrounding catalyst bead.

Figure 6-2 (a) Wheatstone bridge, R_s is the pellistor. (b) alternative arrangement for feedback control to maintain a constant pellistor temperature.

Figure 6-3 (a) Simple micromachined pellistor substrate, showing a meander heater on a Si_3N_4 diaphragm. (b) micromachined pellistor with separate heater, and catalyst layer. [Reprinted from (Gall, 1993) with permission from Elsevier Science]

Figure 6-4 Data based on the dual sensor developed by Zanini et al. The resistance difference between the active and the reference temperature sensing elements of the microcalorimeter plotted as a function of propylene, propane, hydrogen, and carbon monoxide concentration by volume. The right axis shows the corresponding average temperature rise produced by the reaction on the membrane. [Reprinted from (Zanini et al., 1995) with permission from Elsevier Science]

Figure 6-5 Image of sample and reference calorimeter. [Reprinted from (Furjes et al., 2005) with permission from Elsevier Science]

Figure 6-6 Microdifferential scanning calorimeter (a) bare device. (b) coated with Pd catalyst on the sample side. (c) schematic of device layout, with thermocouple junctions on the sample and reference side and a separate heater for each side. [Reprinted from (Cavicchi et al., 2004) with permission from Elsevier Science]

Figure 6-7 Thermal image of calorimeter with a variable width heater to improve temperature uniformity. [Reprinted from (Aigner et al., 1996) with permission from Elsevier Science]

Figure 6-8. Thermal images of the active area for four different microheater designs. [Reprinted from (Lee et al., 2003) with permission from Elsevier Science]

Figure 6-9 Frames from thermal image movie showing initial heating and subsequent cooling from a $40 \mu\text{s}$ that was pulse applied to the upper heater of the microcalorimeter shown in Figure 6-6. Associated graph is the optical signal from the area indicated by the crosshairs converted to a temperature. The optical signal was captured by an oscilloscope triggered before the start of the pulse by $10 \mu\text{s}$ for (a) and (b) and 2ms for (c) and (d). Times for the images from the start of the pulse are (a) 1.5 s , (b) 38 s , (c) 1.9 ms , and (d) 3.9 ms . [Reprinted from (Cavicchi et al., 2004) with permission from Elsevier Science]

Figure 6-10 (a) Thermal image of an operating micromachined calorimeter with an evident cold spot (b) investigation with a scanning electron microscope revealed a hollow

area within the catalyst coating. [Reprinted from (Furjes et al., 2005)with permission from Elsevier Science]

Figure 6-11 Characterization of the oxidation and reduction of a Pd film on alumina by XPS. Shown are the Pd 3d peaks for treatments as indicated. [Reprinted from (Hoogers et al., 1992) with permission from Elsevier Science]

Figure 6-12. XPS survey spectra of (a) clean platinum ribbons, (b) and (c) after exposure to 6.7×10^{-7} mol HMDS at 905 and 995 K respectively. [Reprinted from (Ehrhardt et al., 1997) with permission from Elsevier Science]

Figure 6-13. Normalized signal pattern vs. the working temperatures of a set of eight thermistor calorimeters (measured concentrations between 1 ml/l and 7ml/l in air). [Reprinted from (Riegel and Haerdtl, 1990) with permission from Elsevier Science]

Figure 6-14 Response of a micromachined calorimeter to four gases as a function of inverse temperature. [Reprinted from (Gall, 1993) with permission from Elsevier Science]

Figure 6-15 Signal shapes in air, methanol, ethanol and isopropanol with a modulation frequency 10 Hz [Reprinted from (Aigner et al., 1996) with permission from Elsevier Science]

Figure 6-16 Signal shapes in air, methanol, ethanol and isopropanol with a modulation frequency 10 Hz (After Aigner) Figure 6-16. Temperature profile of an individual scan during the exposures to different gases and concentrations. Concentrations were increased by factors of 2 from the minimum. The traces for each gas show increasing signal amplitude with increasing concentration. For each gas, the range of concentrations was: (a) methanol 12 μ mole/mole (12 ppm) to 200 μ mole/mole (200 ppm), (b) ethanol 6 μ mole/mole (6 ppm) to 100 μ mole/mole (100 ppm), (c) hydrogen 12 μ mole/mole (12 ppm) to 200 μ mole/mole (200 ppm), (d) benzene 6 μ mole/mole (6 ppm) to 100 μ mole/mole (100 ppm), and (e) acetone 6 μ mole/mole (6 ppm) to 100 μ mole/mole (100 ppm). [Reprinted from (Cavicchi et al., 2004) with permission from Elsevier Science]

Figure 6-17 Flow-through design for mounting a pellistor. [Reprinted from (Dabill et al., 1987) with permission from Elsevier Science]

Figure 6-18 (a) Image showing a microheater mounted into a TO can, the lid of which has a diffuser and activated carbon filter integrated. (b) Sensor response for different packaging configurations. [Reprinted from (Norman et al., 2003)with permission from Elsevier Science]

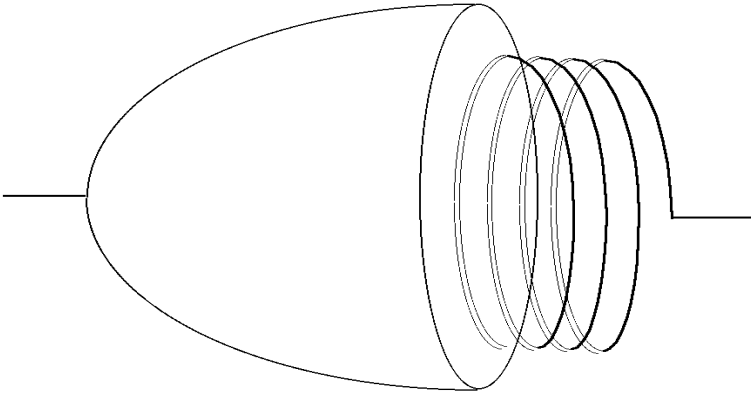


Figure 6-1. Cutaway illustration of a conventional pellistor device, showing the Pt heater wire and surrounding catalyst bead.

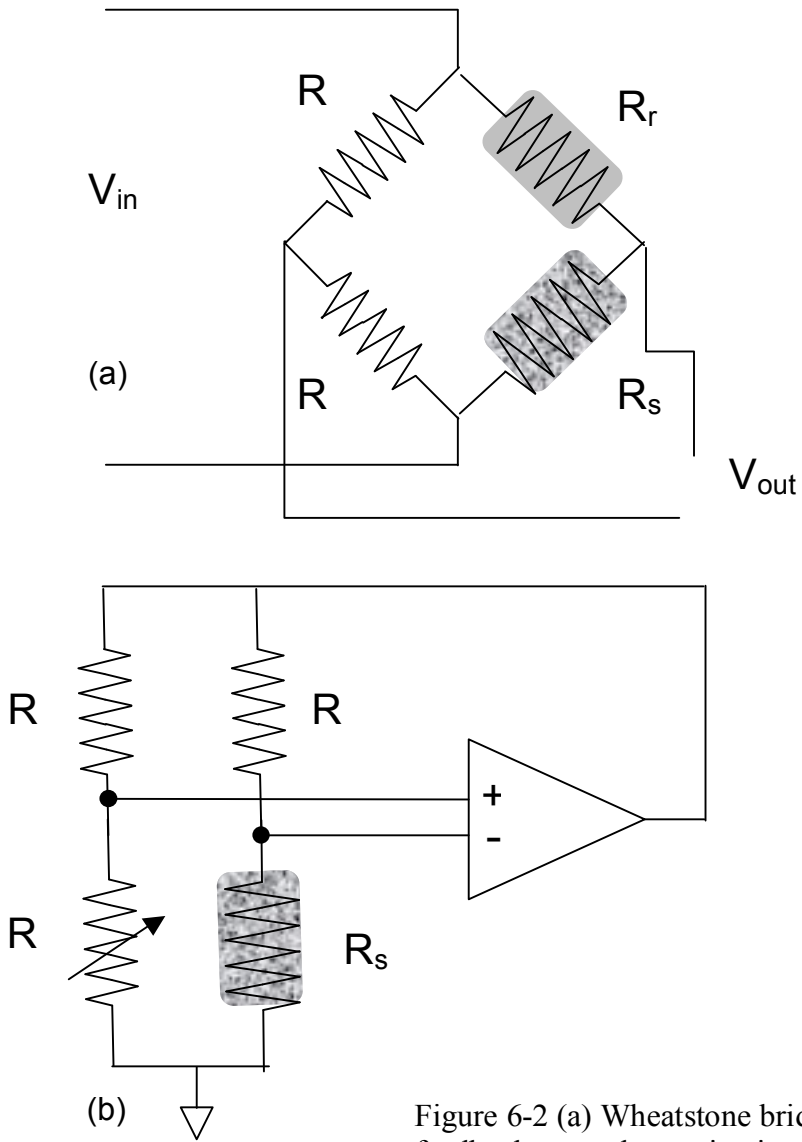


Figure 6-2 (a) Wheatstone bridge, R_s is the pellistor. (b) alternative arrangement for feedback control to maintain a constant pellistor temperature.

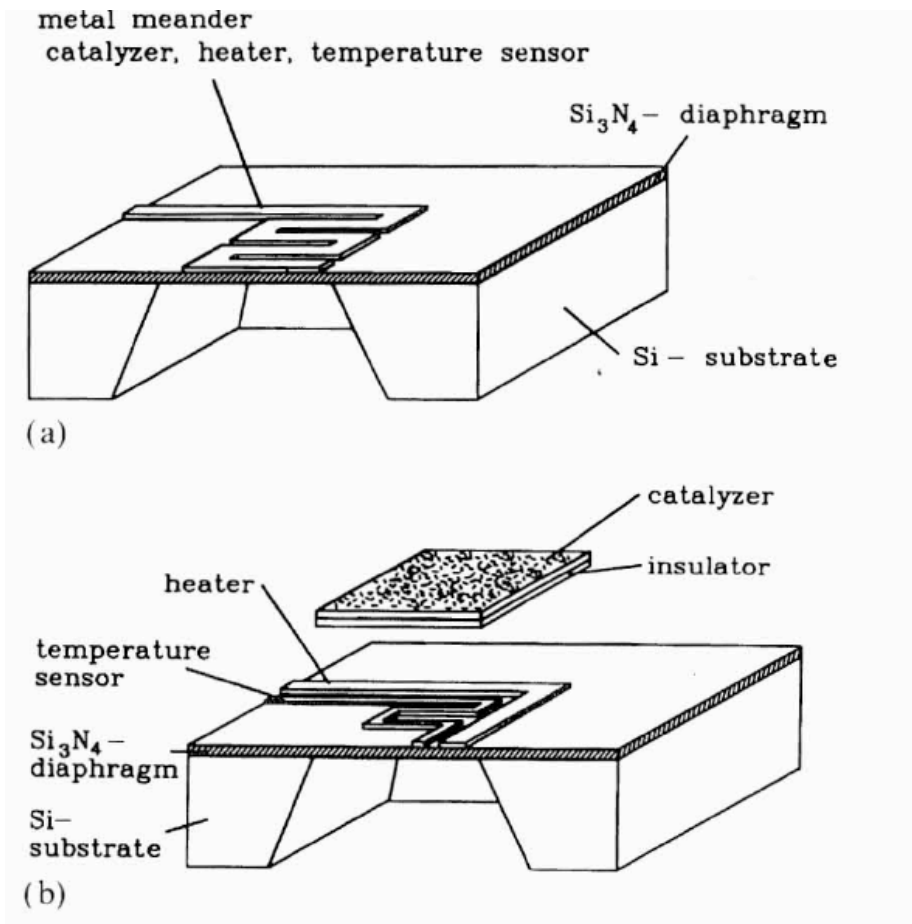


Figure 6-3 (a) simple micromachined pellistor substrate, showing a meander heater on a Si_3N_4 diaphragm. (b) micromachined pellistor with separate heater, and catalyst layer. [Reprinted from (Gall, 1993) with permission from Elsevier Science]

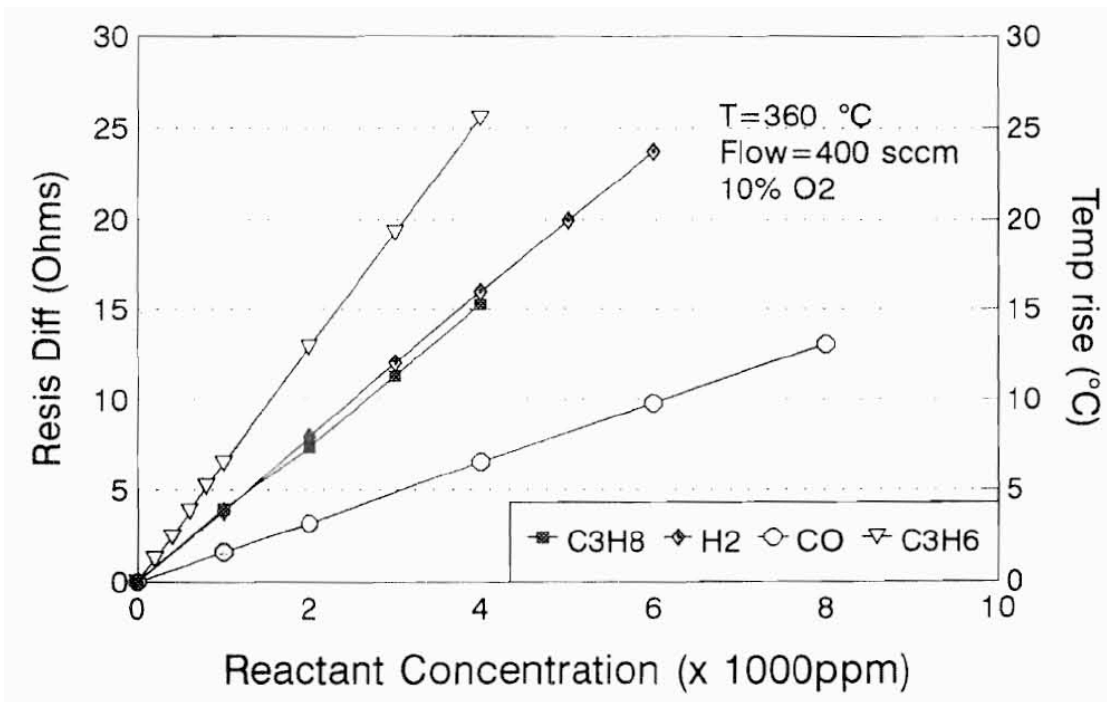


Figure 6-4 Data based on the dual sensor developed by Zanini et al. The resistance difference between the active and the reference temperature sensing elements of the microcalorimeter plotted as a function of propylene, propane, hydrogen, and carbon monoxide concentration by volume. The right axis shows the corresponding average temperature rise produced by the reaction on the membrane. [Reprinted from (Zanini et al., 1995) with permission from Elsevier Science]

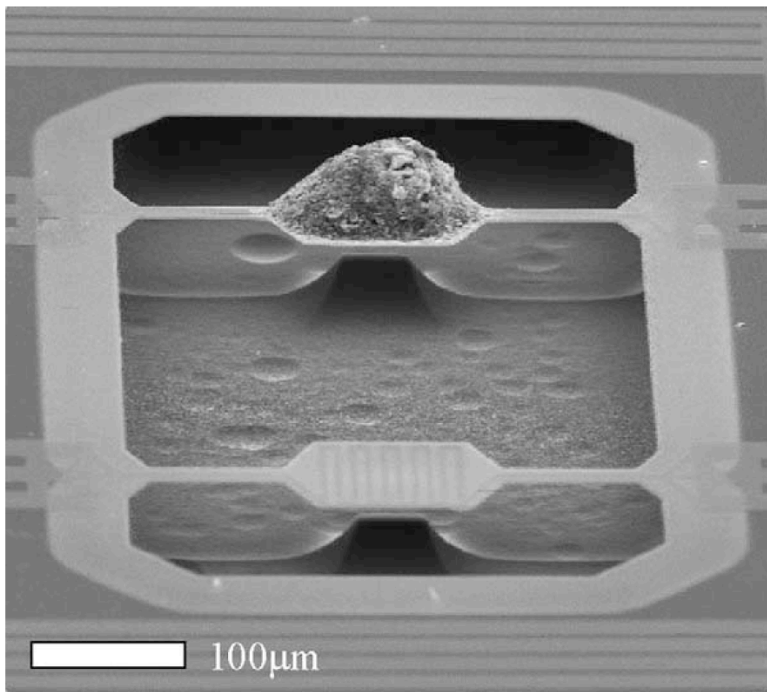


Figure 6-5 Image of sample and reference calorimeter. [Reprinted from (Furjes et al., 2005) with permission from Elsevier Science]

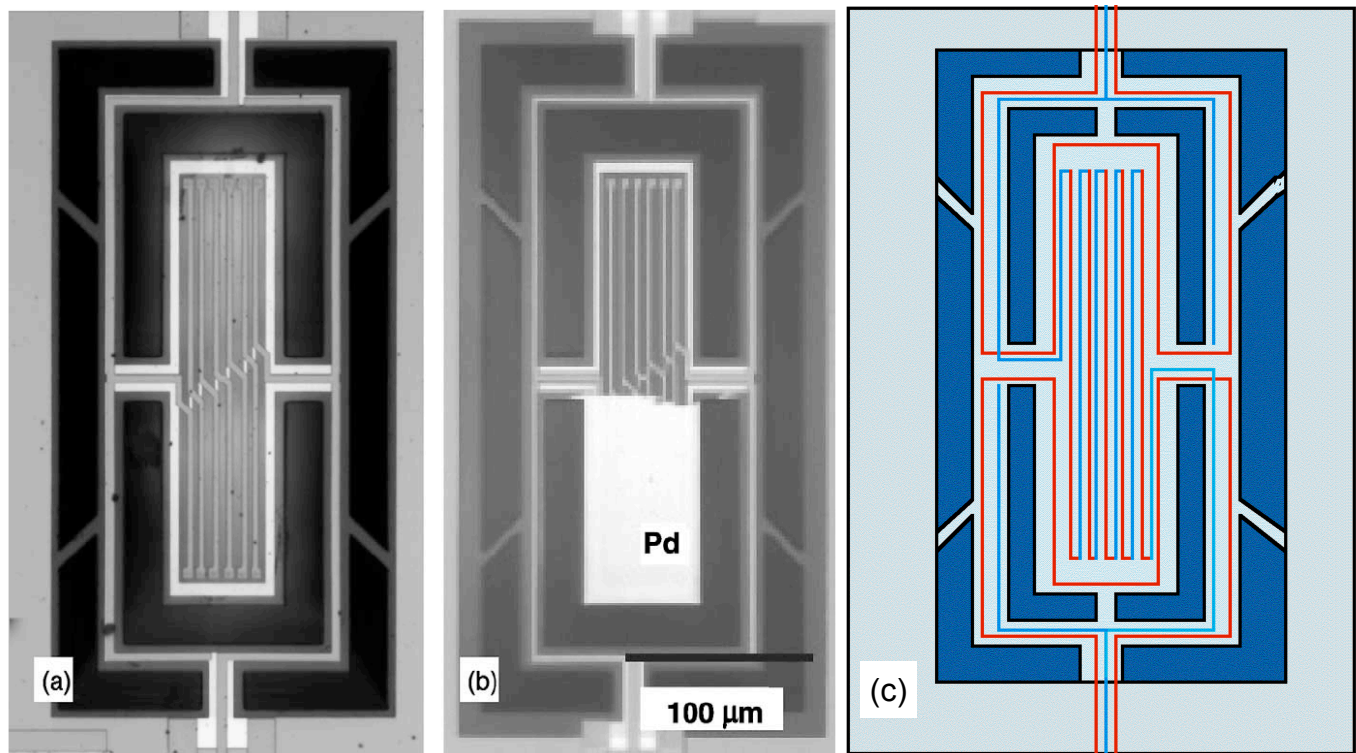


Figure 6-6 Microdifferential scanning calorimeter (a) bare device. (b) coated with Pd catalyst on the sample side. (c) schematic of device layout, with thermocouple junctions on the sample and reference side and a separate heater for each side. [Reprinted from (Cavicchi et al., 2004) with permission from Elsevier Science]

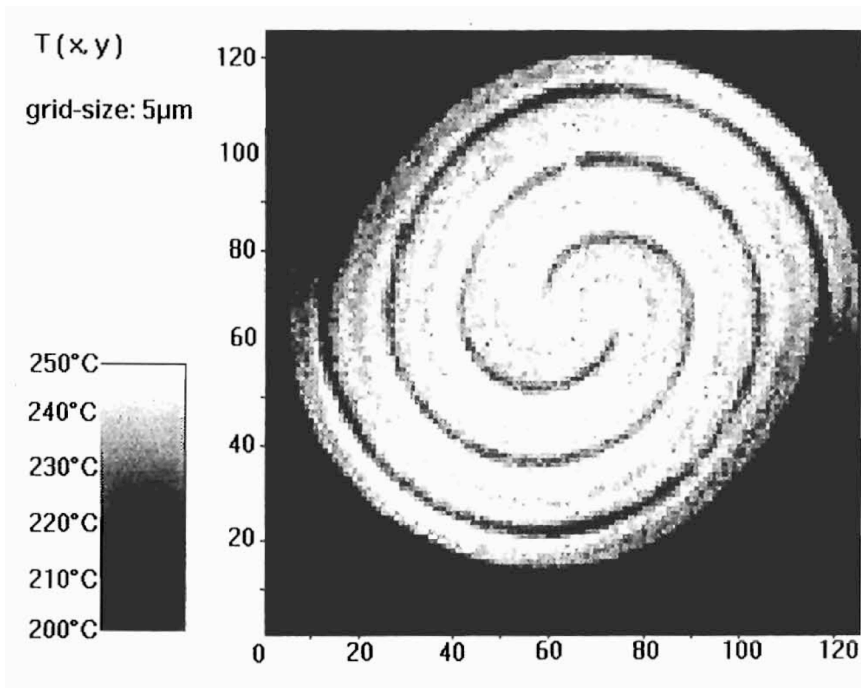
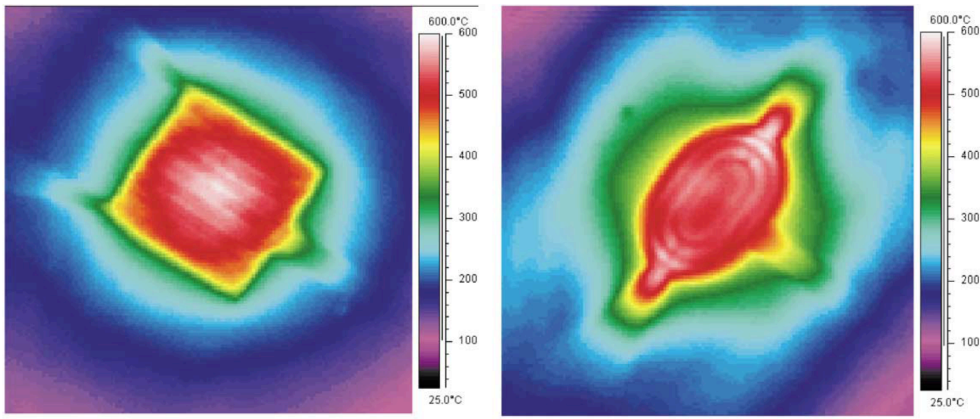
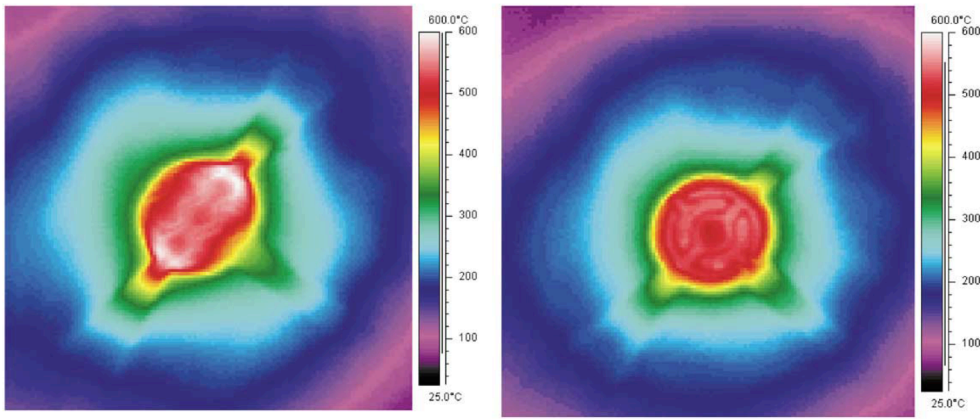


Figure 6-7 Thermal image of calorimeter with a variable width heater to improve temperature uniformity. [Reprinted from (Aigner et al., 1996) with permission from Elsevier Science]



(a)

(b)



(c)

(d)

Figure 6-8. Thermal images of the active area for four different microheater designs. [Reprinted from (Lee et al., 2003)with permission from Elsevier Science]

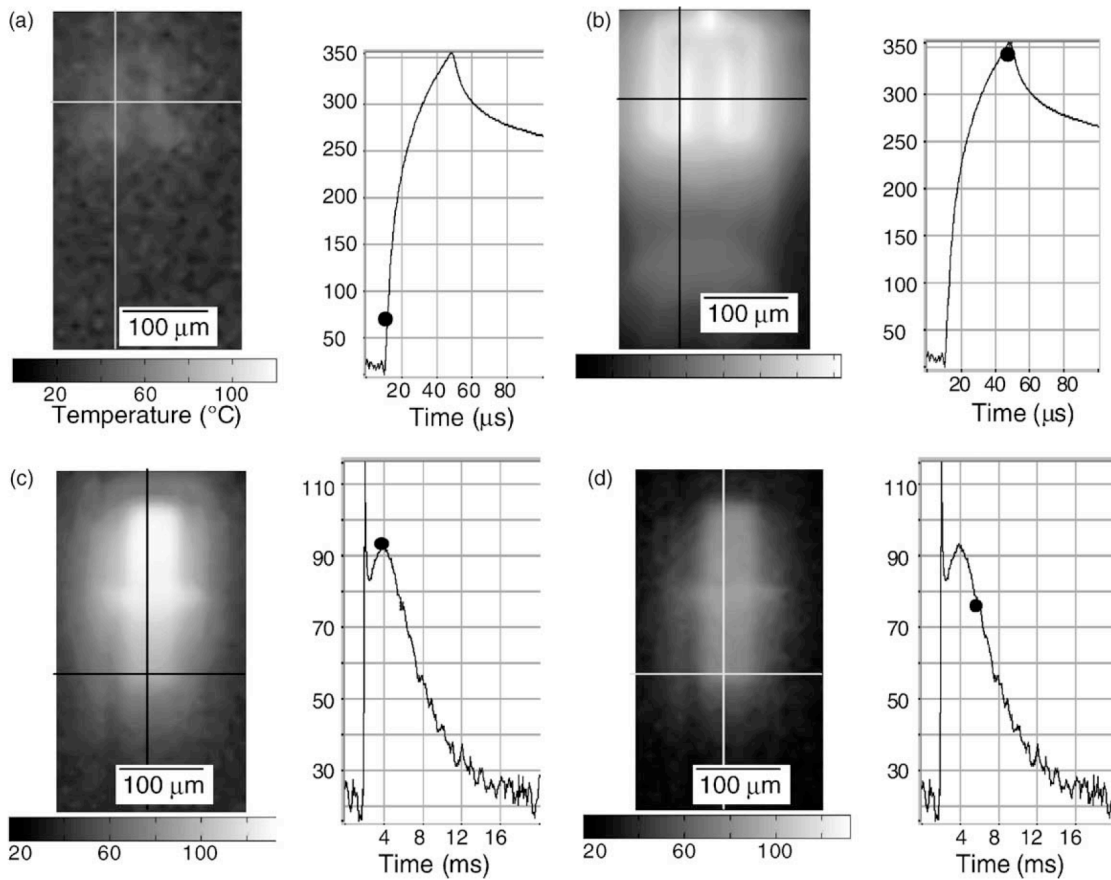
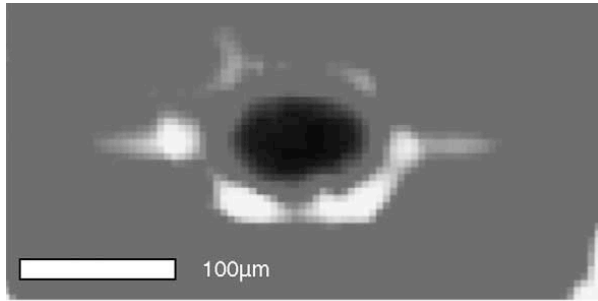


Figure 6-9 Frames from thermal image movie showing initial heating and subsequent cooling from a 40 μs that was pulse applied to the upper heater of the microcalorimeter shown in Figure 6-6. Associated graph is the optical signal from the area indicated by the crosshairs converted to a temperature. The optical signal was captured by an oscilloscope triggered before the start of the pulse by 10 μs for (a) and (b) and 2ms for (c) and (d). Times for the images from the start of the pulse are (a) 1.5 s, (b) 38 s, (c) 1.9 ms, and (d) 3.9 ms. [Reprinted from (Cavicchi et al., 2004) with permission from Elsevier Science]

(a)



(b)

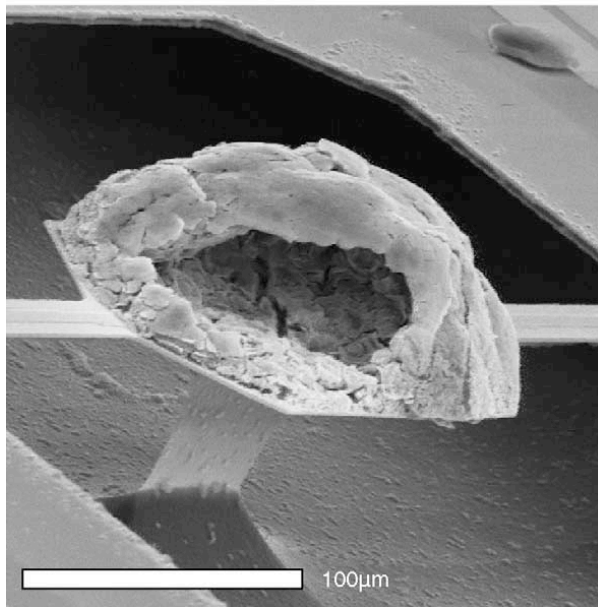


Figure 6-10 (a) Thermal image of an operating micromachined calorimeter with an evident cold spot (b) investigation with a scanning electron microscope revealed a hollow area within the catalyst coating. [Reprinted from (Furjes et al., 2005) with permission from Elsevier Science]

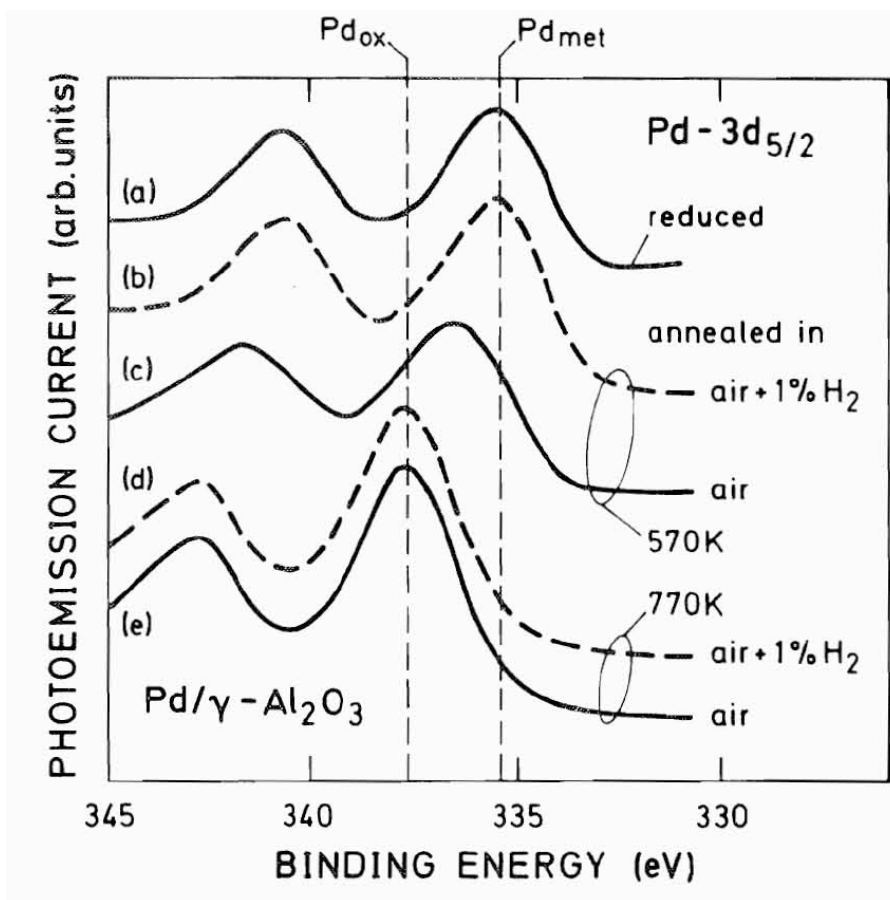


Figure 6-11 Characterization of the oxidation and reduction of a Pd film on alumina by XPS. Shown are the Pd 3d peaks for treatments as indicated. [Reprinted from (Hoogers et al., 1992) with permission from Elsevier Science]

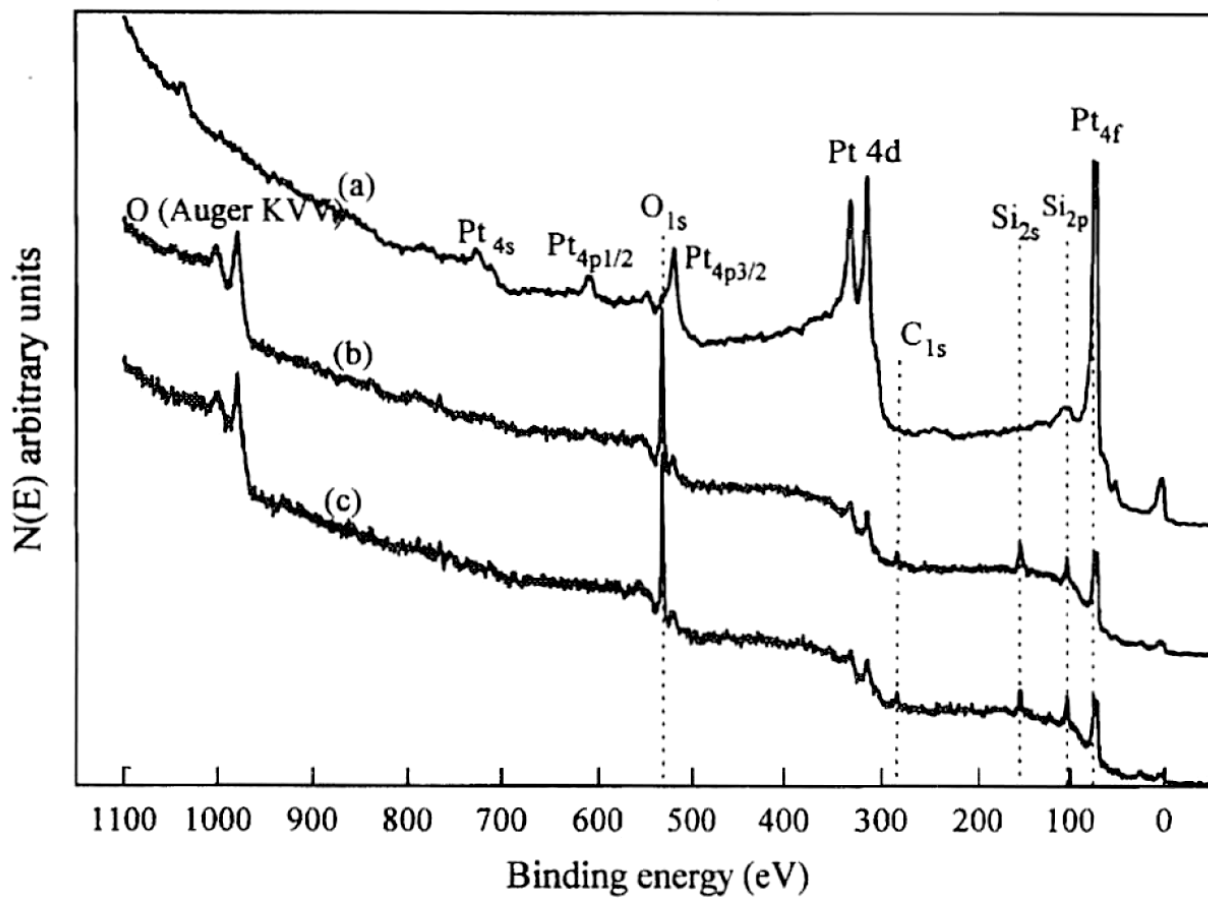


Figure 6-12. XPS survey spectra of (a) clean platinum ribbons, (b) and (c) after exposure to 6.7×10^{-7} mol HMDS at 905 and 995 K respectively. [Reprinted from (Ehrhardt et al., 1997) with permission from Elsevier Science]

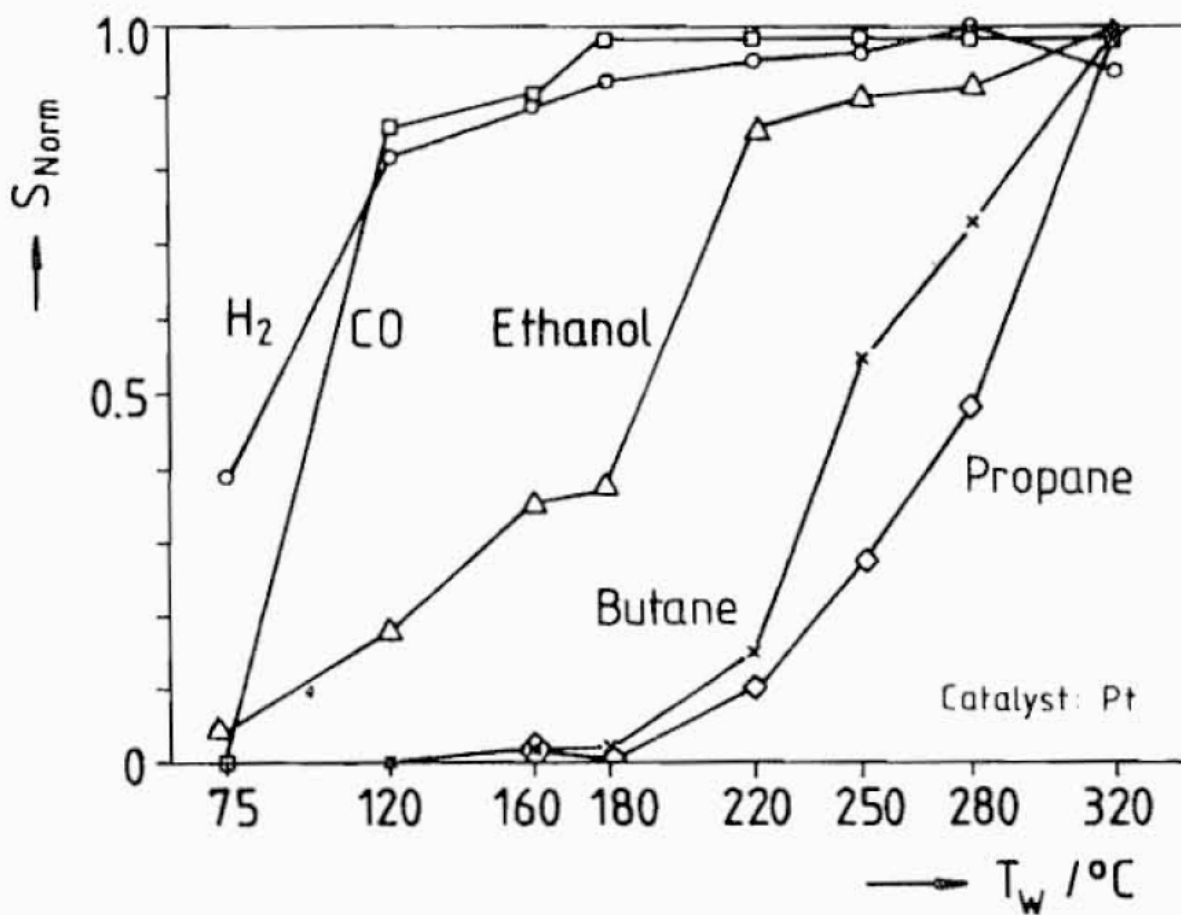


Figure 6-13. Normalized signal pattern vs. the working temperatures of a set of eight thermistor calorimeters (measured concentrations between 1 ml/l and 7ml/l in air). [Reprinted from (Riegel and Haerdtl, 1990) with permission from Elsevier Science]

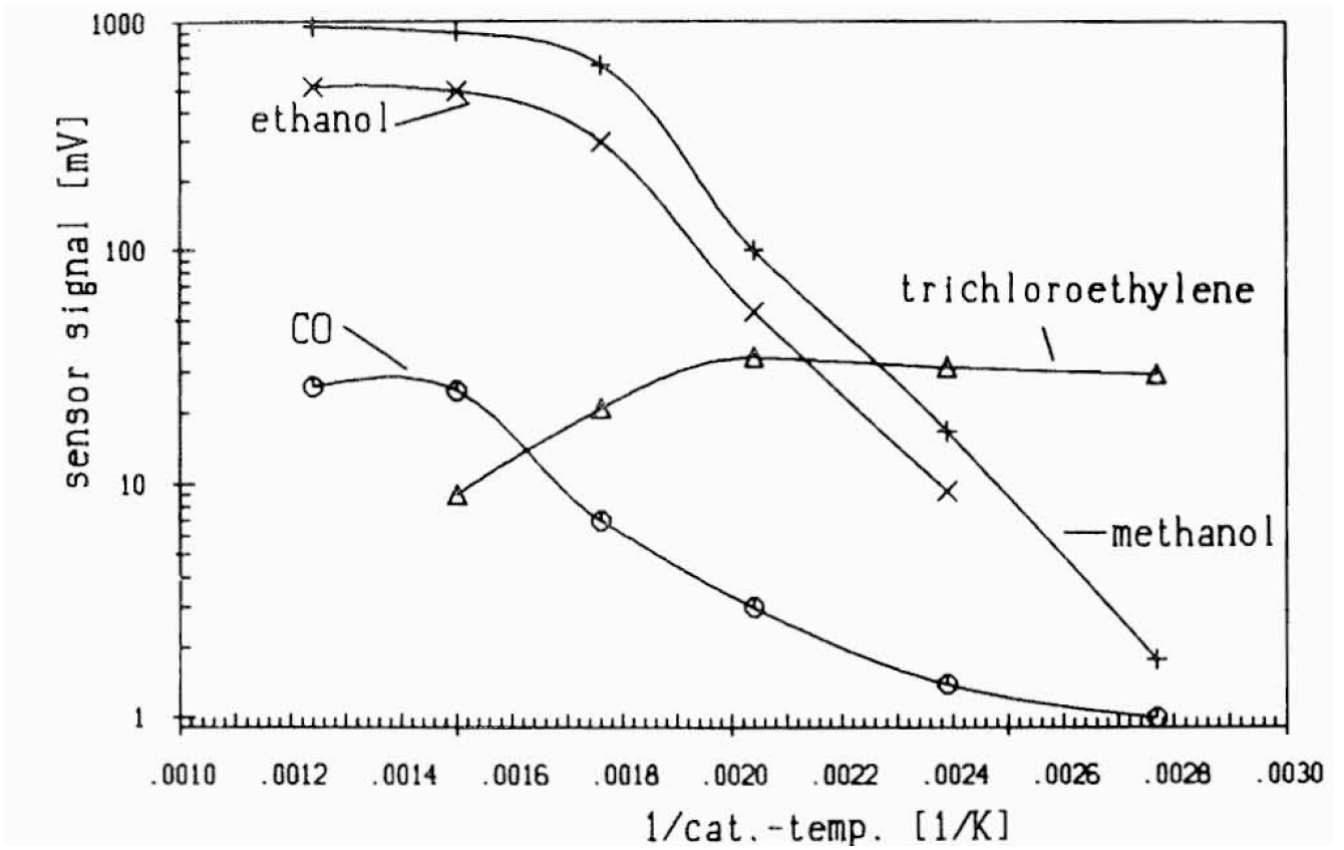


Figure 6-14 Response of a micromachined calorimeter to four gases as a function of inverse temperature. [Reprinted from (Gall, 1993) with permission from Elsevier Science]

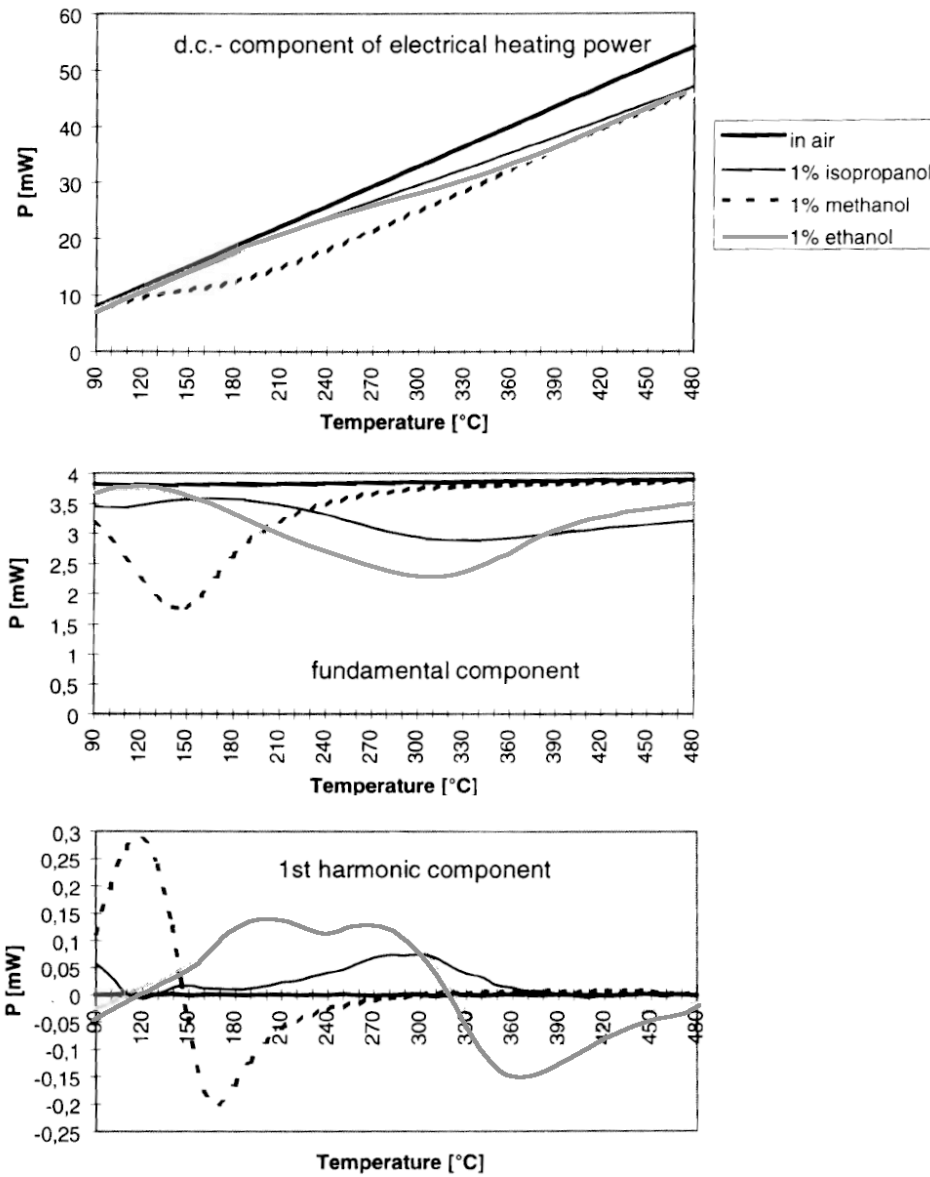


Figure 6-15 Signal shapes in air, methanol, ethanol and isopropanol with a modulation frequency 10 Hz [Reprinted from (Aigner et al., 1996) with permission from Elsevier Science]

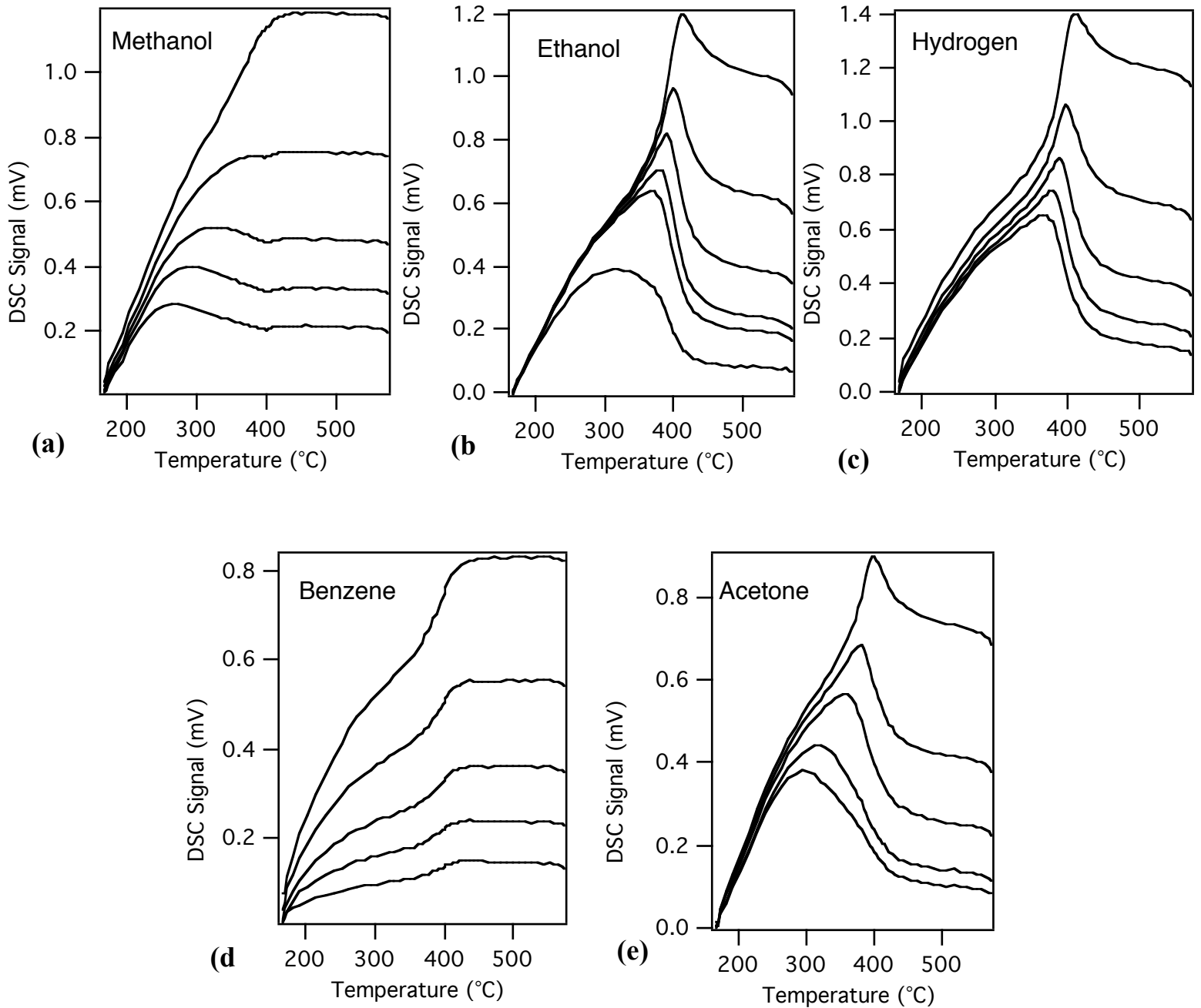


Figure 6-16. Temperature profile of an individual scan during the exposures to different gases and concentrations. Concentrations were increased by factors of 2 from the minimum. The traces for each gas show increasing signal amplitude with increasing concentration. For each gas, the range of concentrations was: (a) methanol 12 mmole/mole (12 ppm) to 200 mmole/mole (200 ppm), (b) ethanol 6 mmole/mole (6 ppm) to 100 mmole/mole (100 ppm), (c) hydrogen 12 mmole/mole (12 ppm) to 200 mmole/mole (200 ppm), (d) benzene 6 mmole/mole (6 ppm) to 100 mmole/mole (100 ppm), and (e) acetone 6 mmole/mole (6 ppm) to 100 mmole/mole (100 ppm). [Reprinted from with permission from Elsevier Science]

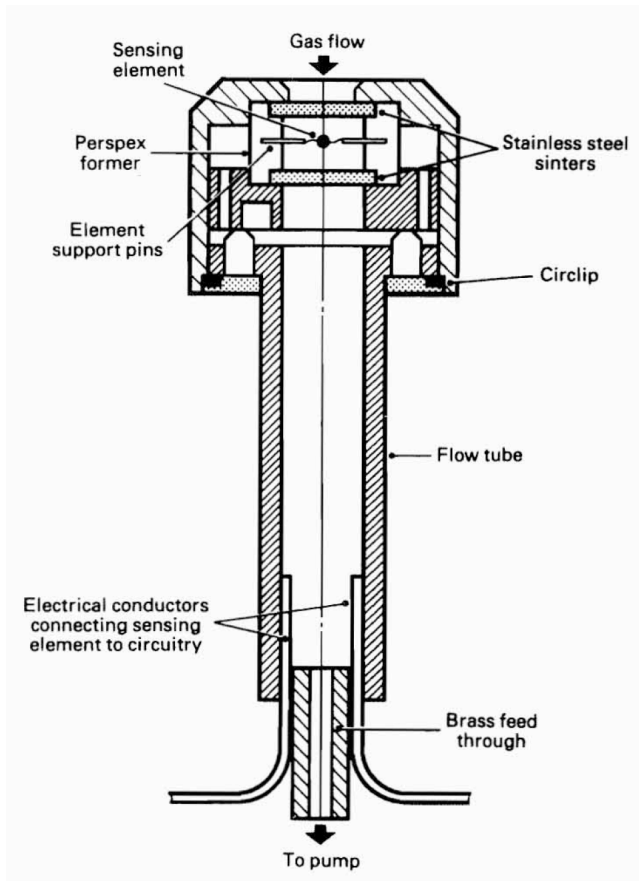


Figure 6-17 Flow-through design for mounting a pellistor. [Reprinted from (Dabill et al., 1987) with permission from Elsevier Science]

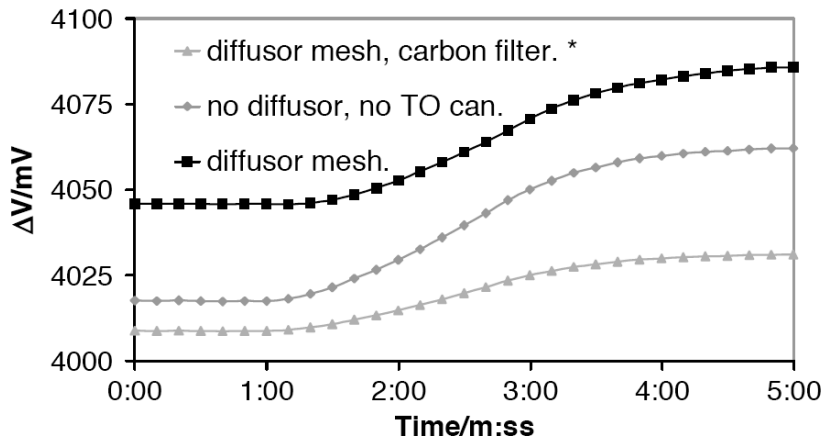
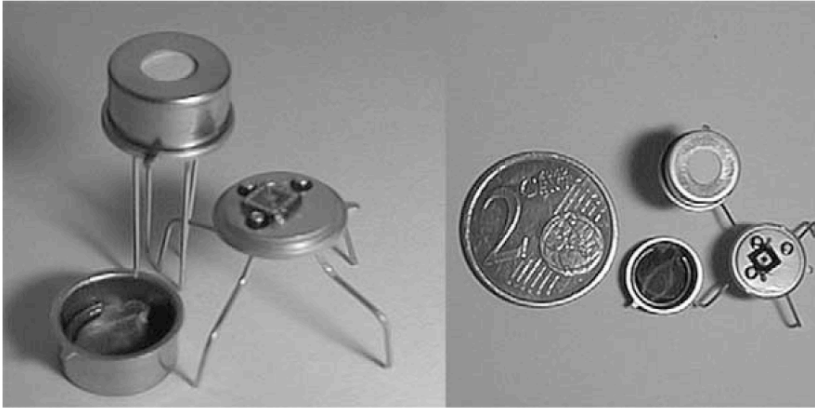


Figure 6-18 (a) Image showing a microheater mounted into a TO can, the lid of which has a diffuser and activated carbon filter integrated. (b) Sensor response for different packaging configurations. [Reprinted from (Norman et al., 2003) with permission from Elsevier Science]

